Trisubstituted Acridines as G-quadruplex Telomere Targeting Agents. Effects of Extensions of the 3,6- and 9-Side Chains on Quadruplex Binding, Telomerase Activity, and Cell Proliferation

Michael J. B. Moore,[†,‡] Christoph M. Schultes,[†,§,‡] Javier Cuesta,[†,||] Francisco Cuenca,[†] Mekala Gunaratnam,[†] Farial A. Tanious,[⊥] W. David Wilson,[⊥] and Stephen Neidle*[,†]

Cancer Research UK Biomolecular Structure Group, The School of Pharmacy, University of London, 29-39 Brunswick Square, London WC1N 1AX, UK, and Department of Chemistry, Georgia State University, Atlanta, Georgia 30303-3083

Received June 13, 2005

The synthesis is reported of a group of 3,6,9-trisubstituted acridine compounds as telomeric quadruplex-stabilizing ligands with systematic variations at the 3-, 6-, and 9-positions. A new microwave-assisted methodology has been developed for trisubstituted acridine synthesis. Structure−activity relationships are reported using surface plasmon resonance and a fluorescence melting assay to examine quadruplex binding, together with a telomerase inhibition assay. These reveal relationships between G-quadruplex stabilization and telomerase inhibition and optimal 3,6- and 9-substituent side-chain lengths for maximal activity. Qualitative molecular modeling using molecular dynamics simulations has been undertaken on four quadruplex−DNA complexes. Long-term exposure of MCF7 cancer cells to a subset of the most active compounds, at doses lower than the IC_{50} values, showed that one compound produced a marked decrease in population growth, accompanied by senescence, which is consistent with telomere targeting by this agent.

Introduction

Telomere status is maintained and regulated in all cells through a complex capping mechanism that prevents chromosomal ends from being recognized as damaged DNA and allows faithful chromosome replication during the cell cycle.[1,2] A host of telomere-associated proteins (including TRF1, TRF2, and POT1) ensure that the telomere, which typically consists of several kilobasepair of double-stranded, G-rich DNA and a 100−200 bp single-stranded overhang on the 3′-strand, does not elicit DNA-damage response pathways or lead to abnormal chromosomal rearrangements.[3−5] Exposure of the 3′-end due to uncapping results in cellular senescence and apoptosis.[6,7]

The enzyme telomerase plays a crucial role in capping assembly.[2,8] It allows the extension of telomeres shortened over successive rounds of replication due to the end-replication effect, and in the absence of this process, telomeres are observed to become critically short after a number of rounds of replication, thus triggering growth arrest and replicative senescence or apoptosis.[9−11] It can thus be seen to work on two levels, the more basic level being templating and extension of the telomere 3′-overhang while the higher level involves more general participation in maintaining telomere homeostasis and other putative roles in DNA-damage signaling pathways.

Telomeres are differentially regulated in normal somatic cells compared to cancer cells, primarily through differing levels of active telomerase enzyme. The correlation between the detection of high levels of active telomerase in cancer cells and its absence or down-regulation in surrounding noncancerous cells has been well established,[12−14] and the activation of telomerase has been identified as one of the key stages in oncogenic transformation.[15] Telomerase function and telomere capping have thus developed into promising targets for anticancer chemotherapies.[16]

In addition to the targeting of the enzyme itself, a number of ways of influencing the DNA substrate of the enzyme itself have been studied, thus opening the way to compounds with a dual role as initiators of telomere uncapping and telomerase inhibitors. These two functions would be expected to result in short-term and long-term effects respectively, by contrast with other types of telomerase inhibition, which have focused on the latter, with attendant problems of an extended time lag.

The single-stranded telomeric overhang which is used by telomerase as a primer during the elongation phase of its action is capable of forming four-stranded DNA G-quadruplex structures.[17,18] In vitro, the use of small molecule ligands to stabilize such structures in DNA sequences mimicking the telomeric 3′-overhang has been shown to result in the inhibition of telomerase activity.[19−23] Furthermore, cell culture experiments with a number of these compounds have been shown to have pronounced effects on cancer cell lines,[24−26] suggesting that stabilization of such structures is incompatible with the correct functioning of telomerase and cancer cell telomere maintenance in general, thereby causing destabilization of the telomere cap and associated processes. The postulated mechanism of action of these compounds is a denial of access to the telomere, both for telomerase and other telomere-associated proteins, such as the length-mediating single-strand-binding protein POT1.[27−29] This can then lead to uncapping,[25] causing chromosomal end-to-end fusions,[30] cell cycle arrest, and growth inhibition. Other studies have also shown that the stabilization of quadruplexes with small molecules hinders the ability of telomere-associated helicases such as BLM and WRN to unwind these higher-order structures,[31−33] again impacting on the correct functioning of the telomere cap. Recent in vivo findings in a mouse xenograft model[34] have demonstrated that exposure to the trisubstituted acridine BRACO19 (**1a**) is associated with tumor growth inhibition and killing of cancer cells, accompanied by atypical mitoses in xenograft tissues, indicative of telomere dysfunction. Analysis showed a loss of nuclear hTERT upon treatment with

* Corresponding author. Tel 44 207 753 5969. Fax 44 207 753 5970. E-mail: stephen.neidle@pharmacy.ac.uk.
† University of London.
‡ These authors contributed equally to this work.
§ Present address: Department of Molecular Oncology, Göttinger Zentrum für Molekulare Biowissenschaften (GZMB), Justus von Liebig Weg 11, 37077 Göttingen, Germany.
|| Present Address: Max Planck Institut für Molekulare Physiologie, Otto Hahn Strasse 11, 44227 Dortmund, Germany.
⊥ Georgia State University.

10.1021/jm050555a CCC: $33.50
Published on Web 12/21/2005

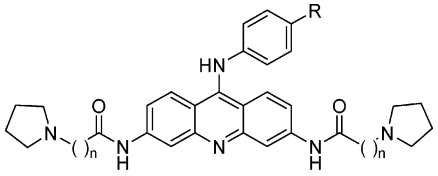

1

Figure 1. Trisubstituted anilinoacridines.

compound and the colocalization of cytoplasmic hTERT with ubiquitin, suggesting that the induced displacement of the enzyme from the telomere targets it for enhanced degradation.

Inhibition of telomerase is thus an important effect associated with telomere-targeting agents, but the full mechanism of action is expected to occur through multiple pathways involving the onset of senescence and apoptosis as well as the elicitation of a DNA-damage response. Although early models of telomerase inhibition suggested that a drawback of telomerase-targeted therapies would be the extended time lag required before telomeres reached critically shortened lengths,[16,35−37a] clear evidence is emerging that G-quadruplex telomere-targeted agents can influence events at the telomere on a much shorter time scale, both in vitro and in vivo.[34,37b]

A large number of mostly planar, aromatic compounds have been shown to be G-quadruplex-stabilizing ligands, including those based on a central acridine scaffold.[19−21] We have previously reported on a number of such trisubstituted acridine analogues with a variety of side-chain modifications and stereoisomer variations, with the best compounds exhibiting strong G-quadruplex binding, high selectivity for quadruplex over duplex DNA, and accompanying telomerase inhibitory activity in the nanomolar range.[19,20,38,39] We present here data from biophysical, biochemical, and cellular studies showing that selective binding of 3,6,9-anilinoacridines (Figure 1) to quadruplex telomeric DNA correlates with telomere targeting and telomerase inhibition and that there are optimal 3-, 6-, and 9-side-chain lengths for maximal activity. In addition to the use of two biophysical methods (FRET and SPR assays) and the biochemical TRAP assay, molecular dynamics simulations were used to examine qualitative structure−activity relationships for interaction with quadruplex DNA, with respect to variations at the 3- and 6-positions.

Results

Chemistry. Following methodology adapted by us to a generic synthesis of **1** ($n = 2$),[20,40] acridines **1e**−**g** (where $n = 2$) were prepared via the key 9-chloroacridine intermediate **11** (Scheme 1). The diaminoacridone **2**[41] was acylated with 3-chloropropionyl chloride followed by amination with pyrrolidine and activation with phosphorus pentachloride and phosphoryl chloride to give **11** typically with an overall yield of 27% over the three steps. Heating a methanolic solution of **7** with the required aniline **15a**−**c**, prepared in a three-step sequence from available 4-nitroaniline, furnished pure **1e**−**g** typically in 55−61% yield from **11** (overall yield from **2** 15−16%) after purification by repeated flash chromatography.

The synthesis of 3,6-extended acridines **1b**−**d** and **1h**−**j** was effected with modifications necessary to dissect differences in reactivity and solubility of acridones (**4**−**6**) and stability of the 9-chloroacridines (**11**−**14**) relative to compounds **7** and **11**, respectively.

Initial attempts at the synthesis of acridones **8**−**10** employed conditions developed for the preparation of **7**.[19] However, these conditions (heating with excess pyrrolidine in ethanol) gave heterogeneous reaction mixtures from which only a small amount of product acridone (2% in the case of **8**) and unreacted starting material were obtained. Use of pyrrolidine as solvent led to complete consumption of the starting material; however, isolation of solid acridone materials from concentrated reaction mixtures by partition between basic aqueous and organic phases proved frustrating and irreproducible at times, as highlighted in the synthesis of **8**, where an oily residue was frequently encountered. Employing cosolvents such as DMF and acetonitrile produced similar results, with hard to manipulate oily residues being produced. Analysis of reaction products by LC/MS indicated peaks [$(M - C_4H_9N)H^+$, $(M - C_4H_9N)H_2^{2+}$, $(M - (C_4H_9N)_2)H^+$, $(M - (C_4H_9N)_2)H^{2+}$] consistent with species arising from elimination of a pyrrolidine fragment (C_4H_9N). Given our concerns regarding the questionable stability of 9-chloroacridines, it was important at this stage of the synthesis to obtain pure acridone. Given the notorious insolubility of acridones, a reputation upheld by **8**−**10**, practical purification methods are limited to washing or recrystallization with alcohol or alcohol/DMF mixtures. These techniques, however, have not proved effective in the purification of acridones **8**−**10**.

The impurities associated with acridones **8**−**10** were found to be transmitted along the synthesis pipeline. Analysis by LC/MS of 9-chloroacridine intermediates **12**−**14** again indicated the presence of elimination products and respective acridone **8**−**10**, which had either remained unreacted or resulted from hydrolysis of the 9-chloroacridine when isolated from the reaction mixture. As feared, the 9-chloroacridines **12**−**14** proved to be unstable, in contrast to **11**, which can be stored, not permitting purification at this point in the synthesis, so **12**−**14** were submitted immediately to the final couplings with excess aniline. Target acridines were found to be thermally labile with elimination of pyrrolidine to provide an olefinic product as observed by ^{1}H NMR analysis. Heating was restricted in the final coupling reaction to apprehend this elimination but with the effect of decreasing reaction efficiency. Crude mixtures were obtained whose components included target acridine, aniline, acridone, and elimination products from which pure target acridines were extruded by repeated flash chromatography. Thus, the series **1b**−**d** (R = $N(CH_3)_2$, $n = 3-5$) and **1h**−**j** (R = 3-(pyrrolidin-1-yl)propionamidoanilino, $n = 3-5$) were prepared in respective overall yields of 1−4% and 2−6% from **2**, which are lower than that observed for the synthesis of 3,6-bis-propionamidoacridines **1e**−**g** ($n = 2$) (overall yield 15−16%).

It was considered that problems associated with this synthetic route may be bypassed by employing a route centered on 3,6-diazido-9-chloroacridine (**16**), readily available from **2** by diazotization and then treatment with thionyl chloride.[42] In a step that introduces the 9-substituent earlier in the synthesis, compound **16** was coupled with the aniline **15b** to give pure 9-substituted diazido acridine (**17**) in 83% yield [cf. an average yield of 13% when introducing the 9-substituent later in the synthesis (Scheme 1)]. Catalytic hydrogenation of **17** proceeded smoothly (67%) to give **18**. With the application of microwave heating, the 3,6-bis(chloroalkylamido) derivatives **19**−**21** were able to be prepared in parallel with yields ranging from 60 to 80%. Reaction with pyrrolidine at only room temperature furnished pure target acridine in an average yield of 57%, after only one round of flash chromatography.

Comparing the two synthetic routes presented, we find that acridines **1h, 1i, 1j** are prepared in higher overall yield (19%, 24%, 9%, respectively) by employing the diazido route (Scheme 2) compared to the 9-chloroacridine route (Scheme 1) (3%, 6%, 2%), which is notable as the diazido route is a longer synthesis

Scheme 1. 9-Chloroacridine Route to 3,6,9-Trisubstituted Acridines[a]

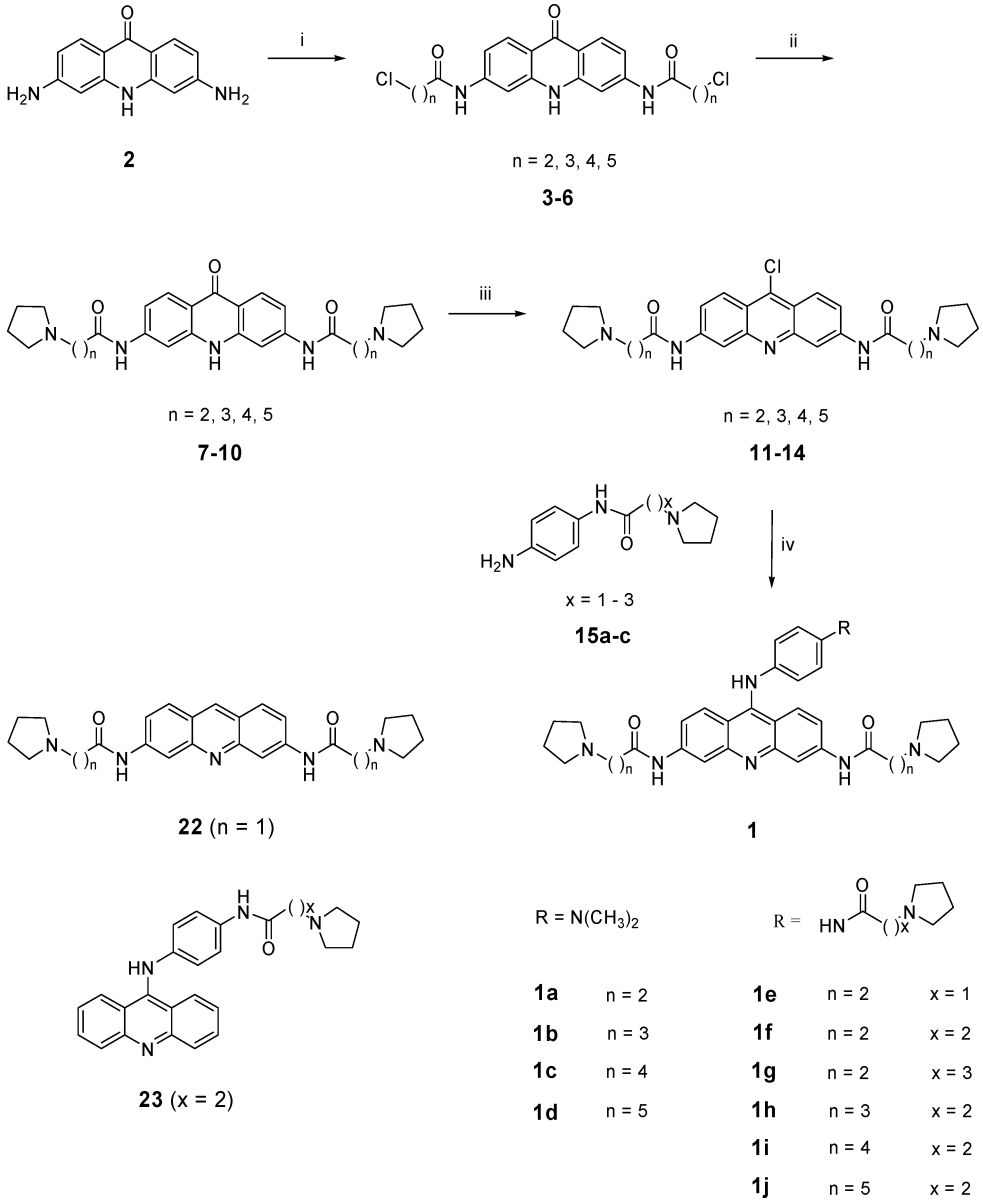

[a] (i) $Cl(CH_2)_{n=2-5}COCl$, 80 °C; (ii) pyrrolidine, Δ; (iii) PCl_5, $POCl_3$, Δ; (iv) 15a−c or *N*,*N*-dimethylaminoaniline, MeOH, Δ.

by two steps. In addition, the diazido route is advantageous as cleaner chemistries are employed.

FRET Assays of Quadruplex Binding. The melting curves obtained for compounds **1a**−**d** were all of the same shape with a major transition, yielding a $[conc]_{\Delta T_m=20°C}$ value and a small, minor transition occasionally observed at lower temperatures (Table 1). Only the major melting transitions are reported here, as the smaller transitions were not large enough to yield consistently accurate temperature measurements. For the main melting step, the trend across the series was one of decreasing quadruplex stabilization with increasing side-chain length.

Comparing FRET results for extended acridines **1a**−**d** and **1e**−**j** has been hampered by the inconsistent shape of some melting curves, which may be quantified by the poor correspondence between ΔT_m and $[conc]_{\Delta T_m=20°C}$ values. In some cases it is difficult to discern obvious trends. For 3,6-bis-propionamido acridines modified at the 9-position, **1e**−**g**, there is a slight increase in ΔT_m with 9-substituent length that plateaus, although such a trend does not hold when comparing the $[conc]_{\Delta T_m=20°C}$ parameter.

In terms of the 3,6-extended analogues **1f** and **1h**−**j**, the 3,6-bis-butanamido derivative **1h** gave a relatively low FRET value (ΔT_m = 22.63 °C), whereas the shortest 3,6-bis-propionamido derivative **1f** and longest 3,6-bishexanamido derivative **1j** showed the greatest stabilization. The 9-modified acridines **1e** and **1g** compare well with the 3,6-modified acridines **1i** and **1j** and have markedly higher ΔT_m values than **1h**.

TRAP Assays of Telomerase Activity. Compounds **1a** and **1b** both show sub-micromolar inhibition of telomerase activity, in agreement with an earlier study on **1a**.[19,20] The $^{tel}EC_{50}$ value for this compound reported here (113 nM) is within experimental error of the two previously reported values (95 and 115 nM, respectively). A large decrease in telomerase inhibitory activity was found with increasing side-chain elongation (Table 1). This closely parallels the trend in the FRET assay data for these four compounds but is much more striking in the TRAP data, with **1c** and **1d** exhibiting $^{tel}EC_{50}$ values of 1.9 and 6.9 μM, respectively.

Acridine **1f** was found to be the most potent telomerase inhibitor ($^{tel}EC_{50}$ = 67.4 nM) of the compounds presented in

Scheme 2. Diazido Route to 3,6,9-Trisubstituted Acridines[a]

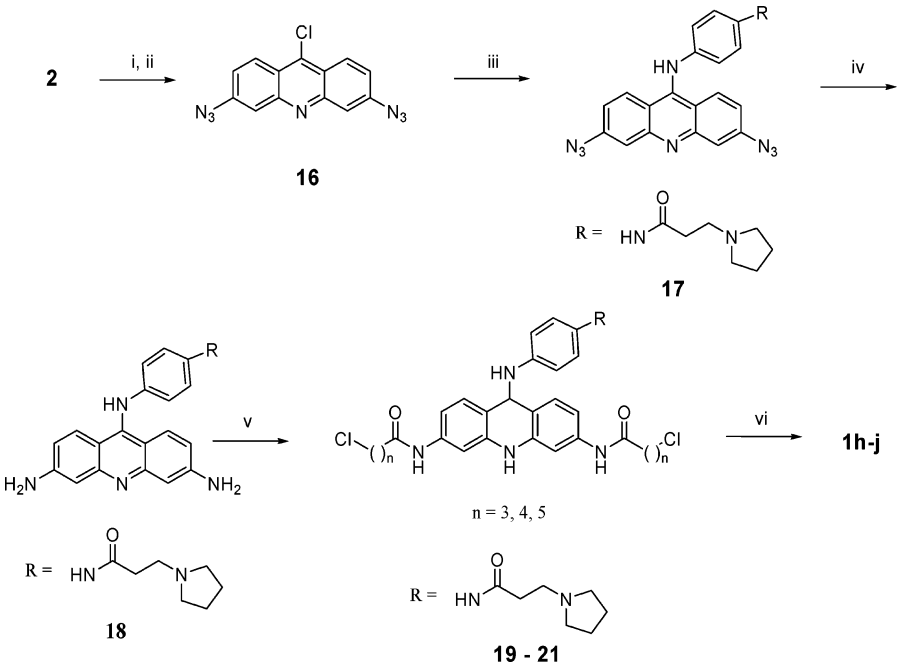

[a] (i) $NaNO_2$, dilute H_2SO_4, NaN_3, 0 °C to rt; (ii) $SOCl_2$, rt; (iii) **15b**, catalytic HCl, NMP; (iv) H_2 20 psi, 10% Pd−C, MeOH/EtOAc; (v) $Cl(CH_2)_{n=3-5}COCl$, TEA, toluene, μW; (vi) pyrrolidine, rt.

Table 1. Quadruplex FRET and TRAP Data[a]

compd	$\Delta T_m(1\mu M)$ (°C)	$[conc]_{\Delta T_m=20°C}$ (μM)	error (μM)	$^{tel}EC_{50}$ (nM)	error (nM)
1a	27.5	0.7	0.1	113	1
1b	16.5	1.1	0.1	99	2
1c	6.8	2.1	0.1	1930	320
1d	4.7	2.6	0.1	6910	1400
1e	34.8	0.3	0.02	167	16.1
1f	37.6	0.1	0.01	67	1.5
1g	37.9	0.3	0.01	117	7.9
1h	22.6	0.7	0.08	326	16.1
1i	36.2	0.3	0.01	255	23.3
1j	39.3	0.3	0.00	146	1.8
22	14.6	2.5	0.4	5200	nd
23	5.5	13.8	1.7	>20000	nd

[a] $\Delta T_m(1\mu M)$, change in melting temperature at 1 μM drug concentration; $[conc]_{\Delta T_m=20°C}$, concentration of compound required to effect a 20 °C change in melting temperature; $^{tel}EC_{50}$, concentration of compound required to achieve 50% inhibition of telomerase inhibition; nd, not determined

Table 2. SPR Data[a]

compd	K_{dsDNA} ($\times 10^6$ M^{-1})	K_{G4DNA} ($\times 10^6$ M^{-1})	ratio (K_{G4DNA}/K_{dsDNA})
1a	1.0	31.0	31.0
1b	0.1[b]	4.8	48.0
1c	0.4	1.8	4.5
1d	0.1[b]	0.6	5.8
1e	6.8	74.0	10.9
1f	1.0	29.0	29.0
1g	6.0	77.0	12.8
1h	5.0	3.0	0.6
1i	0.7	1.1	1.6
1j	0.3	18.0	72.0
22	1.1	1.3	1.2
23	nd	nd	nd

[a] Fitting errors for determination of K with a particular SPR data set are ±5%. Experimental errors in K based on reproducibility in repeat experiments are ±20% for the quadruplex studies. K_{dsDNA}, binding constant of compound to double-stranded DNA; K_{G4DNA}, binding constant of compound to quadruplex DNA; K_{G4DNA}/K_{dsDNA}, ratio of K_{dsDNA} to K_{G4DNA}; nd, not determined. [b] Note that values of K_{dsDNA} for **1b** and **1d** are upper limits. Thus K_{G4DNA}/K_{dsDNA} values are likely to be greater than 48 and 5.8, respectively.

this study. A propionamide-based linker in the 9-position is optimal in this series, as the compounds with a longer 9-position side chain [**1e** (acetamide) and **1g** (butanamide)] have potencies a factor of 2 worse than **1f**. Analogous to the observations in the FRET studies, **1h** shows a significant decrease in inhibitory potency, which nevertheless improves as the 3- and 6-side chains become longer, although the effect is more pronounced in the TRAP than in the FRET assay. Acridines **1e** and **1g** are roughly equipotent with **1j** ($^{tel}EC_{50}$ values of 100−200 nM). Interestingly, compound **1i**, which displays similar G4 DNA stabilization as **1f**, is a less potent telomerase inhibitor. Telomerase inhibition correlates well overall with the FRET data, providing evidence for the utility of this technique in screening the potency of potential telomerase inhibitors.

Surface Plasmon Resonance Studies of Quadruplex Affinity. SPR yields direct information on the binding of the ligands to both the human quadruplex and duplex DNA and thus enables the determination of the ratio of the two equilibrium-binding constants (K_{G4DNA}/K_{dsDNA}; Table 2), which is a measure of G-quadruplex binding selectivity. In the concentration range examined, ligands bound significantly more tightly to quadruplex DNA and had slower kinetics than binding to duplex DNA, in particular with respect to dissociation (Figure 2a,b). As can be seen for compound **1a** in Figure 2b, the duplex curves reached a steady-state plateau soon after injection of the compound. With the quadruplex, however, at the lowest concentrations, it took significantly longer to reach a steady state plateau (Figure 2a; note the different time scales in parts a and b of Figure 2). The association reactions are bimolecular with rates that are concentration-dependent, but the first-order dissociation reactions can be directly compared. The kinetics differences between the duplex and quadruplex reactions are apparent in the plots. The steady-state RU (response units) values were determined in the plateau regions of the sensorgrams and are plotted versus the free compound concentration (from the flow solution) in Figure 2c. Fitting of binding curves using

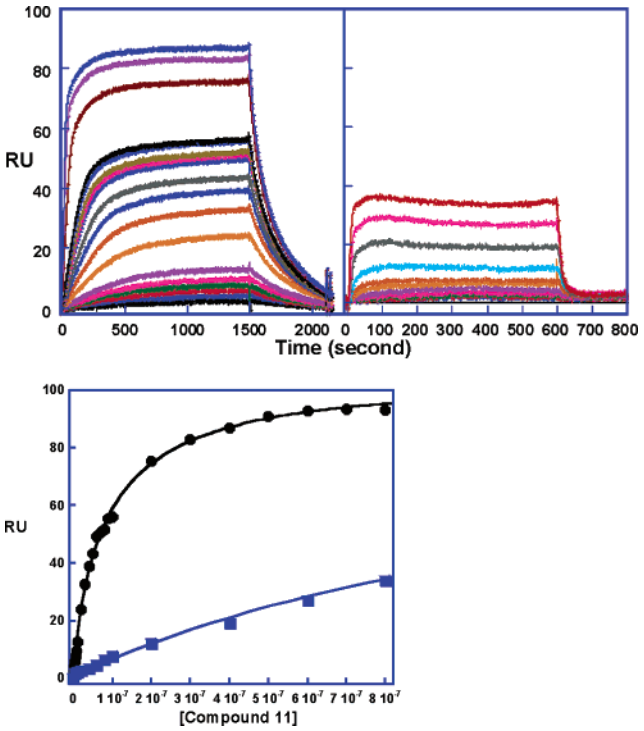

Figure 2. (a, b) SPR sensorgrams for the interaction of compound **1a** with the human telomere G-quadruplex hairpin DNA (a, left) as well as a duplex hairpin with a CGAATTCG stem sequence (b, right) are shown. The concentrations of the compounds increase from 1×10^{-9} M (lower curve) to 8×10^{-7} M (highest curve) in both plots. The experiments were conducted at 25 °C in HEPES buffer with 200 mM K^+. (c) Binding isotherms are shown for compound **1a** with the -AATT- duplex (blue squares) and G-quadruplex (black circles) and were constructed with results from experiments such as those in a and b. The RU values from the steady-state region of the sensorgrams were plotted versus the concentration of the compounds. The lines in the figures were obtained by nonlinear least-squares fits of the data to a two-site-binding model.

a two-binding-site model suggests that the acridines all had a single strong binding site on the quadruplex with a weaker secondary binding interaction associated with a 10−20-fold lower affinity. This weaker interaction could not be accurately evaluated in the experimental concentration range and only the stronger binding constants are reported here. With the other compounds, the kinetics of quadruplex dissociation are faster and the RU values at each concentration are significantly lower than with **1a**. Sensorgrams for **1b** are shown as examples in the Supporting Information. The faster dissociation of **1b** relative to **1a** can be seen, and the duplex shows very little binding of **1b**. The duplex binding constants for **1b** and **1d** are quite low and are upper limit estimates.

All *K* values determined by the steady-state method are given in Table 2. K_{dsDNA} values are in a smaller range (from 1×10^5 to 6.8×10^6 M^{-1}) compared to K_{G4DNA} values, which showed greater variation, from 6×10^5 M^{-1} (for **1d**) to 7.7×10^7 M^{-1} (for **1g**). Elongation of the 3- and 6-side chains significantly decreased quadruplex affinity, both in the group of compounds containing an uncharged 9-side chain (**1a**−**d**) and in the set containing the charged terminal pyrrolidine group at the 9-position (**1e**−**j**). The ratio of quadruplex-to-duplex binding was still very favorable for **1b**, due to its diminished duplex affinity; however, this effect is even more noticeable for the 3,6-hexanamido derivative **1j**, which due to its low dsDNA affinity displayed the best quadruplex selectivity of all the ligands studied here. This suggests that in general the added steric bulk of these ligands at the 3- and 6-positions is both unfavorable for quadruplex binding and detrimental to duplex affinity. Conversely, **1e** and **1g** exhibit the largest values for K_{G4DNA} but show lower ratios due to an increase in duplex binding. The importance of duplex−quadruplex selectivity and the favorable effect of trisubstitution was also evident when all the 3,6,9-acridines studied were compared to the disubstituted analogue **22**, which demonstrated a roughly equal affinity for both forms of DNA (Table 2).

Experiments on quadruplex binding kinetics were also performed with **1a**, although only sensorgrams at lower concentrations that are dominated by the single strong binding site were analyzed. As the kinetics for binding to duplex DNA were too rapid to be accurately assessed by SPR methods, only quadruplex binding was examined. Both the association and dissociation rates were lower for the acridine−quadruplex interaction than for the corresponding acridine−duplex complex, but the larger affinity constants for quadruplex DNA were mainly derived from the effect on the dissociation kinetics. The binding constants calculated using the kinetics methods were within experimental error of those determined by steady-state measurements (data not shown).

Molecular Modeling. Molecular dynamics simulations were performed on four G-quadruplex ligand complexes, with compounds **1a**−**d** (Figure 3a−d). An initial simulation for the native quadruplex resulted in an average rmsd value of 1.59 Å for the DNA residues 1−21 over the whole trajectory, which is similar to the rmsd for the loop residues (average rmsd 1.52 Å). The rmsd of the G-quartets remained steady and low throughout the course of the simulation, with an average value of 0.58 Å, in accordance with previous reports on long-term quadruplex simulations.[43−45] The TTA loops, on the other hand, showed much higher variation, again in accord with previous simulation studies.[45,46]

The MD runs for the four ligand complexes showed that the presence of the ligand has only a minor impact on the flexibility of the quadruplex structure, apart from compound **1d**. Its longer side chains make favorable contacts with the loops, thereby reducing the flexibility of the DNA backbone at those positions. The behavior of the quadruplex−**1a** complex illustrates two phenomena that have a significant impact on quadruplex flexibility. The rotational barrier for the C−N bond between the acridine and the 3- and 6-substituted amide appears to be relatively low, and the amide can therefore "reverse" (with respect to the starting conformation) into a conformation whereby the carbonyl oxygen faces toward the center of the uppermost quartet rather than away from it. This causes a shift in the entire side chain and subsequently in the chromophore position, resulting in a tighter "crescent" shape for the 3,6-acridine, forcing the substituent in question to make new contacts with the DNA. Although this did not result in major changes in quadruplex structure, it indicates that the pyrrolidine−phosphate interactions made by the 3,6-side chains are not very stable and can be influenced by intramolecular changes in conformation, possibly due to nonoptimal side-chain length.

Conformational changes in the loops also have an impact on ligand position. As was seen for the native quadruplex, the loop regions relaxed during the simulation and lost some of their initial structure, accounting for their generally larger rmsd. As the three TTA loops expanded during the simulations, the C5 methyl groups of the thymines tended to become more deeply buried within the pocket, thereby making the groove on the ligand-facing side of the loop shallower and displacing the pyrrolidine group of the ligand. This caused disruption of the

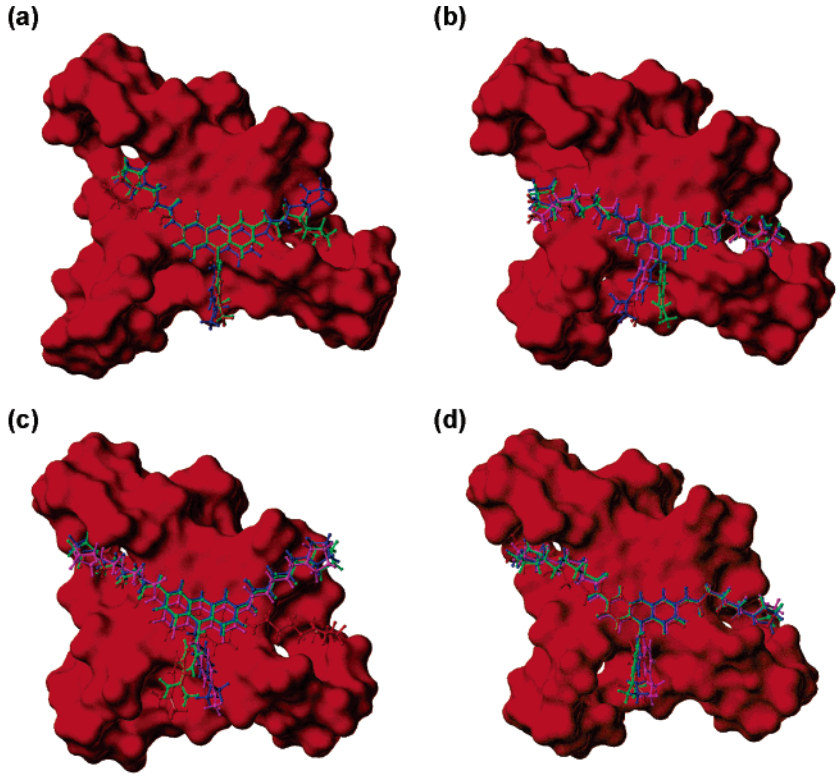

Figure 3. Average (minimized) structures extracted from particular segments of the MD simulations for the ligand−DNA complexes containing compounds **1a,b**. Segments were chosen upon visual inspection of the trajectories. (a) **1a**, red (0−375 ps), green (500−575 ps), blue (925−1000 ps); (b) **1b**, red (0−200 ps), green (250−400 ps), blue (500−650 ps), magenta (700−900 ps); (c) **1c**, red (0−150 ps), green (375−550 ps), blue (575−700 ps), magenta (875−975 ps); and (d) **1d**, red (200−300 ps), green (350−450 ps), blue (675−750 ps), magenta (800−950 ps).

loop contacts made by the 3- and 6-substituents, and although the third loop demonstrated equivalent motion, the 9-substituent was not buried deeply enough in the pocket to be affected.

Elongation of the side chains by one methylene with respect to **1a** (ie compound **1b**) appeared to overcome both of these problems to some extent, as the differing 3- and 6-side chains make contacts that are neither affected by the loop thymines nor prone to the amide reversal observed for **1a**. Further increases in the length of the side chains to give compounds **1c** and **1d** caused greater variation in the ligand motion on the quadruplex surface due to the greater flexibility of the 3- and 6-side chains (Figure 3c,d). It was noticeable for **1c** that the conformation of one of the 3,6-substituents differs with respect to both **1a** and **1b**. The greater length caused it to straighten out and probe the loop more thoroughly, whereas the shorter groups of both the latter compounds caused interactions close to the upper lip of the groove. Furthermore, for **1a**−**c** the tight binding of one of the 3,6-side chains was usually offset by looser binding of the other substituent to the loop with which it was in contact, accompanied by a correspondingly increased fluctuation over the course of the simulation. With **1d**, the longer 3,6-side chains made tighter interactions with the DNA loops, and the ligand position was considerably more stable over the course of the simulation, as can be seen for averaged snapshots taken during the experiment (Figure 3d).

Cell Biology Studies. Long-term cell viability studies were undertaken on two compounds, representative of the most potent telomerase inhibitors in each subgroup, **1a**−**d** and **1e**−**j.** Cellular responses to exposure were examined in order to establish short-term cytotoxicity profiles prior to these studies. The sulforhodamine B (SRB) assay is a widely used method for the assessment of cellular chemosensitivity in a high-throughput format.[47,48] The upper threshold level of cytotoxicity at which cell death is the result of general, and irreversible, cell damage can be determined by the calculation of an IC_{50} value. Those for **1b** were 8.75 μM in the MCF7 breast carcinoma cell line and >25 μM in the IMR90 noncancer fibroblast line. In the latter cell line, compound **1a** showed a similar lack of toxicity (IC_{50} > 25 μM), while results from six different tumor cell lines have been previously determined for it (the average IC_{50} is 10.6 ± 0.7 μM).[24] Compound **1f** exhibited a small decrease in cell growth over the 96-h assay period, although 50% cytotoxicity was not reached in the concentration range examined and the IC_{50} values in the MCF7 and IMR90 cell lines were thus >25 μM. For all other compounds with 3,6- and 9-position modifications, IC_{50} values were ≫25 μM in the MCF7 and IMR90 cell lines.

A series of long-term studies was undertaken in order to assess the effects of selected compounds when administered at concentrations below the IC_{50} values. Compound **1b** produced a large decrease in the rate of population growth in 4-week exposure experiments, even at concentrations considerably below its IC_{50} value in the MCF7 cell line (Figure 4a). At a 5 μM concentration, cell numbers were insufficient after the third week for a continuation of the experiment, with a drop in the cell number recorded after week 2. At 2 μM, a delayed effect was observed, with the number of population doublings falling significantly after 2 weeks, and even at 1 μM exposure, a discernible difference was observed between the control and treated cells. The rate of population growth remained relatively low thereafter, although there were indications that the cells may have started to recover after days 21−28.

Compound **1f** produced only a minor decrease in the short-term growth rate of MCF7 cells with respect to vehicle controls (Figure 4c), despite being a significantly more potent telomerase inhibitor, as judged by its $^{tel}EC_{50}$ value. As in previous

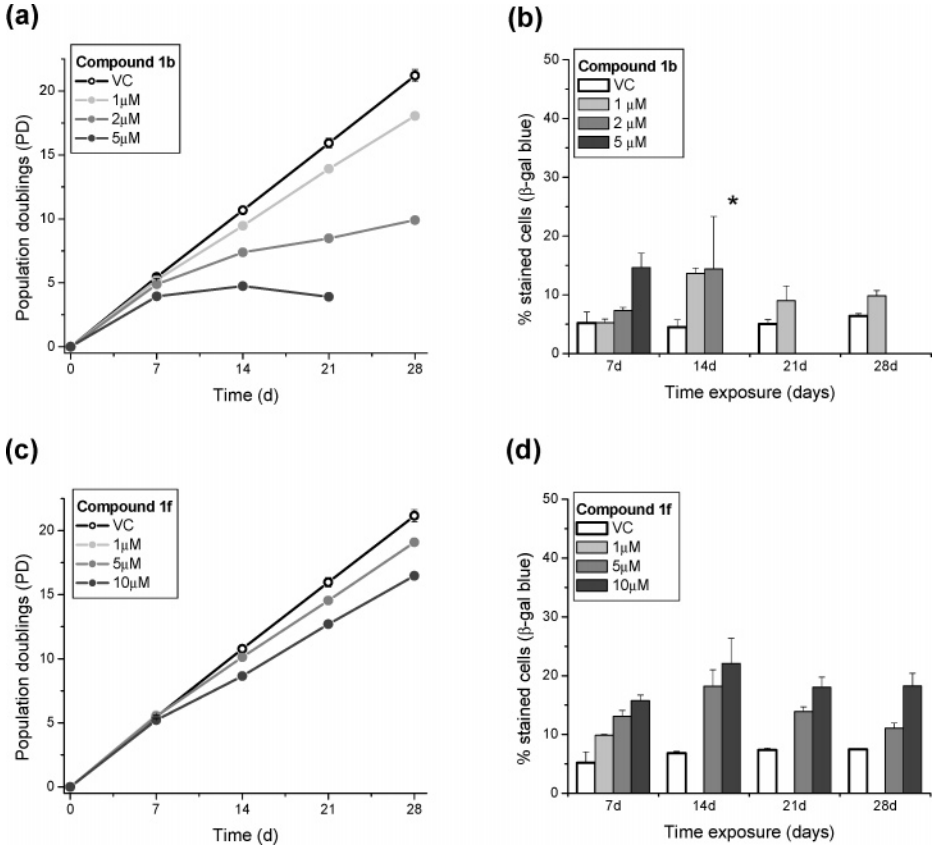

Figure 4. (a). Plot of population doublings (PD) against time for cellular exposure to compound **1b** (three separate concentrations; VC, vehicle control). Long-term (4-week) cell growth experiments for **1b** were performed using the breast adenocarcinoma cell line MCF7, with cells exposed twice per week and counting carried out weekly. (b) Percentage of total cells counted staining for senescence-associated β-galactosidase (SA-β-Gal) activity upon long-term (4-week) exposure to **1b** at varying concentrations. ***** indicates that counting of stained cells following exposure to **1b** was difficult due to the shrunken morphology of the cells; see the text for further details. (c) Plot of population doublings (PD) against time for cellular exposure to compound **1f** (three separate concentrations; VC, vehicle control). Long-term (4-week) cell growth experiments for compound **1f** were performed using the breast adenocarcinoma cell line MCF7, with cells exposed twice per week and counting carried out weekly. (d) Percentage of total cells counted staining for senescence-associated β-galactosidase (SA-β-Gal) activity upon long-term (4-week) exposure to **1f** at varying concentrations. Cells were stained once per week following twice-weekly exposure.

experiments, no effect was observed in the first week of exposure and the overall divergence from the controls was not large. However, a decrease in the proliferation rate was noted after the second week at 5 and 10 μM concentrations, although the results suggest that after 3−4 weeks the growth rate of the exposed cells was gradually returning to pre-exposure levels.

Senescence was estimated with the SA-β-Gal assay, in parallel with the long-term tissue culture studies, using a fraction of cells set aside after counting. The number of cells stained for senescence thus corresponds directly to the data recorded in the plots describing the population doubling behavior of the cell populations. A clear increase in the percentage of cells staining for SA-β-Gal was observed with respect to controls, even at a 1 μM concentration for compound **1b** (Figure 4b). At higher concentrations, staining and counting of the SA-β-Gal expressing fraction was affected by the morphology of the cells following exposure. At 2 μM and above, shrunken, shriveled cells were observed, making it difficult to distinguish the characteristic blue coloration upon staining. Cells staining for SA-β-Gal were observed to show localized staining in the nucleus, the intensity of color ranging from faint at low compound concentrations to increasingly intense as the amount of compound was increased. Additionally, populations exposed to compound displayed a proportion of stained cells exhibiting an enlarged and flattened morphology that has been described as a characteristic feature accompanying senescence,[49,50] as well as a tendency for the fraction of stained cells to be higher in regions of dense clustering. This may be due to paracrine effects associated with the expression of senescence-inducing genes in cells that have already undergone senescence themselves.[51]

Analogous four-week experiments carried out with **1f** were insufficient to establish any significant trends in senescence staining over longer time periods. An increase in the number of cells staining for senescence was initially observed after which cell populations treated with 10 μM compound consistently showed around 20% senescent cells (Figure 4d). The corresponding values at 1 and 5 μM were lower, decreasing to just above vehicle control levels after 28 days. This supports the gradual return to control proliferation rates at these concentrations after 3−4 weeks as observed in the growth rate experiments. Morphologically, no shrinkage or distortion of normal cell shape was observed even after 4 weeks of treatment with **1f**, and staining was consistent with what was observed for compound **1b**.

Discussion

Biophysical and in Vitro Assays. The biophysical FRET and SPR assays, together with the TRAP assay, all show that the side-chain length in this series of trisubstituted acridines is optimal for quadruplex binding and telomerase inhibition when $n = 2$ or 3 (i.e., compounds **1a** and **1b**, respectively). Additionally, the effect of the third, 9-position substituent on

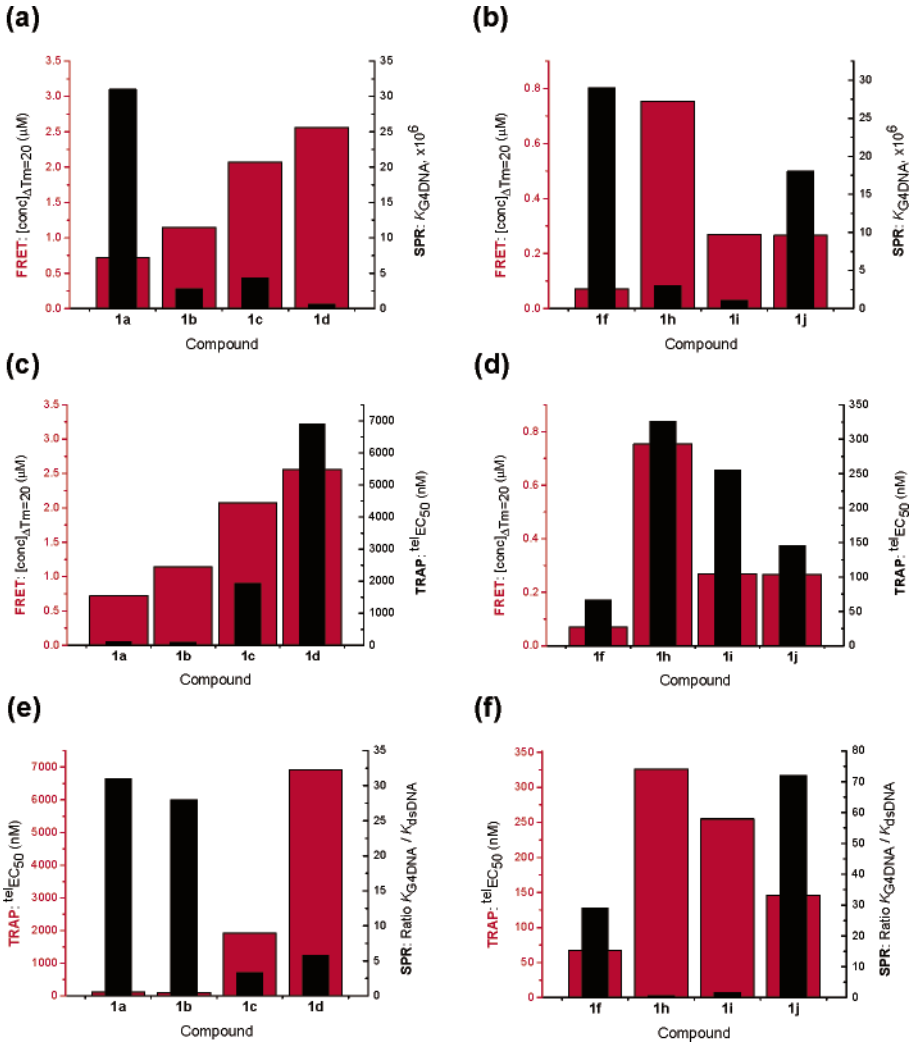

Figure 5. Biophysical correlations for compounds **1a**−**d** and **1e**−**j**. (a, b) FRET−SPR correlations; comparisons of $[\text{conc}]_{\Delta T_m=20°C}$ and K_{G4DNA} would be expected to show an inverse correlation, with strong quadruplex binders demonstrating low FRET values (red bars) and high SPR values (black bars). (c, d) FRET−TRAP correlations; changes in $[\text{conc}]_{\Delta T_m=20°C}$ and $^{tel}EC_{50}$ values should be directly proportional, with potent compounds showing both low FRET values (red bars) and TRAP values (black bars). (e, f) TRAP−SPR correlations; as with the FRET−TRAP correlation, a favorable K_{G4DNA}/K_{dsDNA} ratio (black bars) translates into increased telomerase inhibition in the TRAP assay (black bars). $\Delta T_m(1\mu M)$, change in melting temperature at 1 μM drug concentration; $[\text{conc}]_{\Delta T_m=20°C}$, concentration of compound required to effect a 20 °C change in melting temperature; $^{tel}EC_{50}$, concentration of compound required to achieve 50% inhibition of telomerase inhibition; K_{dsDNA}, binding constant of compound to double-stranded DNA; K_{G4DNA}, binding constant of compound to quadruplex DNA; K_{G4DNA}/K_{dsDNA}, ratio of K_{dsDNA} to K_{G4DNA}.

the acridine scaffold is highly additive, as can be seen for the data obtained for the disubstituted acridine analogue **22**.

We have compared the data derived from the FRET and SPR experiments, since both provide measures of ligand−quadruplex binding affinity. Although the FRET assay gives an indirect estimate of quadruplex binding, since stabilization of the quadruplex may not be directly related to binding affinity, a plot of $[\text{conc}]_{\Delta T_m=20°C}$ against K_{G4DNA} for the ligand set nevertheless shows that they have an inverse proportionality relationship (Figure 5a,b), giving strong support to the use of high-throughput screening of compounds using FRET as an indicator of quadruplex affinity.[39,52] Compound **1f** is the outstanding outlier from this pattern, with anomalously low duplex and quadruplex binding indicated by the SPR studies, which contrast with its high potency in both the FRET and TRAP experiments. The second correlation that we observe is between the FRET and TRAP data. The postulated mechanism of action implies that increased quadruplex stabilization results in more potent telomerase inhibition. This has been found previously for structurally related 3,6,9-trisubstituted acridines,[39] as well as for more structurally diverse molecules, such as indoloquinolines,[52] benzoindoloquinolines,[22] dibenzophenanthrolines,[53] and ethidium derivatives.[54] The data for the present series confirm that an improvement in quadruplex stabilization as determined by FRET corresponds directly to enhanced $^{tel}EC_{50}$ values (Figure 5c,d), again providing support for high-throughput FRET as a screening approach.

Addition of ligand to the DNA probe in FRET experiments was also observed to cause the appearance of a minor melting step prior to the main melting process from which the T_m values are derived in a number of experiments. These compounds thus increase the stabilization of the DNA structure as a whole, yet also cause minor local destabilizing effects. This may be due to interactions with the loop regions, which are likely to be less stable than the central guanine-stacked core and may transmit small effects to the fluorophores through small rearrangements of the G-stacks due to changes in loop topology. The effects of changes in loop structure on quadruplex stability have been investigated using both biophysical[55] and computational[45,46] approaches, and they may have an important impact on quadruplex targeting in the future as compounds designed to interact more efficiently with the quadruplex loop sequences

are investigated. These data also gives some insight into changes in quadruplex structure upon melting and the steps involved in this process. Computational studies have attempted to assess the importance of various intermediates in the folding of quadruplexes,[56] and conversely, some of these processes may be of importance in understanding quadruplex unfolding. One of the principle factors governing quadruplex formation and stabilization is the role of the monovalent cations that coordinate within and between the G-stacks of the quadruplex core.[56−58] Loss of cations from within the core causes significant destabilization of the quadruplex structure. Compounds such as 9-anilinoacridines, which, at physiological pH, contain cationic chromophores capable of interacting with the uppermost G-quartet through "pseudocation" effects,[59] may therefore exert their stabilizing effect partly by blocking, or diminishing, cation loss from between the G-quartets.

In a manner similar to the FRET/TRAP correlation, the relationship between the SPR and TRAP data should be one whereby increased ligand binding affinity for quadruplex DNA corresponds to greater potency in the TRAP assay. However, the TRAP assay contains a PCR step, the efficiency of which is related to the duplex affinity of the compound tested, and it was therefore decided to compare telomerase inhibition data with the quadruplex-to-duplex binding ratio (K_{G4DNA}/K_{dsDNA}), rather than directly with the quadruplex affinity data alone. In this way, the impact of both the K_{G4DNA} and K_{dsDNA} properties of the acridines on the inhibition assay are taken into account. Plots of $^{tel}EC_{50}$ values against the binding ratio confirmed this inversely proportional relationship, and the use of the ratio gave a better correlation than the use of K_{G4DNA} alone (Figure 5e,f). This is especially important in the comparison between compounds **1a** and **1b**. Although the former shows a 10-fold greater affinity for quadruplex DNA compared with the latter, the diminished duplex affinity of **1b** leads to both compounds having comparable K_{G4DNA}/K_{dsDNA} ratios, which is reflected in their similar $^{tel}EC_{50}$ values. This was further underlined by the results of the TAQ inhibition assay, which showed <25% PCR inhibition even at 2 μM for all four trisubstituted acridines examined (**1a**−**d**, data not shown).

The use of a two-binding-site model in the SPR experiments and thus the identification of a weaker binding site to the quadruplex DNA structure may be reflected in the corresponding two-step FRET melting curves noted above. It has been suggested that the two faces of the parallel quadruplex are not energetically equivalent in terms of binding to molecules such as acridines with extended side chains,[19] and it is conceivable that one face presents the major binding site for the compounds examined in this study while the other represents the weaker site. This highlights the varying extents to which the acridine chromophore and the side chains are responsible for the observed quadruplex affinity and ultimately potency against telomerase in the TRAP assay. The final measured affinity is a combination of these two features, with the acridine providing a strong $\pi-\pi$ stacking interaction with the G-quartet while the side chains probe outlying DNA structure. This is confirmed when trisubstituted acridines are compared with disubstituted analogues, and the resulting improvement when going from two to three side chains is due not simply to the decreased duplex binding affinity of the 3,6,9-acridines but also to the increased ligand−DNA interactions that can be attributed to the third moiety. Comparisons between large sets of acridine compounds[19,39] show that correlations are evident among structurally related subseries of compounds, but not among diverse compounds in general. This suggests that large variations in side-chain structure may significantly alter the binding mode of the compounds on the G-quartet surface.

The results presented here highlight a number of structural issues related to ligand−DNA interactions that could usefully be addressed in the further development of 3,6,9-acridines. The choice of initial starting conformation for the ligand G-quartet surface was based on structure−activity relationships (SARs) from previous work[19] and relied on three main assumptions supporting the chosen orientations. First, the three acridine substituents should attempt to contact the three loops of the quadruplex, as it has been shown that modifications at all three positions can cause significant changes in binding affinity and potency.[19,20] Second, a charge on the central nitrogen of the acridine appeared favorable and may assert this influence through positioning directly above the potassium axis that runs through the center of the quadruplex structure, perpendicular to the G-quartets. In this way, it may act as a "pseudo-potassium ion" in the stabilization of the uppermost G-tetrad.[59] Third, only one exposed quartet of the quadruplex was considered as a binding site on the basis of the crystal structure (the "3′-face"). This face is exposed to water, whereas the second (5′) face lies directly adjacent to the same face from a neighboring quadruplex in the crystal packing arrangement and had been suggested to be the more energetically favorable site for binding.[19] It is difficult to judge the extent to which the choice of starting conformation played a role in the MD simulations performed. Genetic algorithm (GA) conformational searches performed during the setup of the ligand−DNA complexes indicated that there was not a significant energetic difference between the lowest energy conformers of the acridines. Changes in ligand position are therefore likely to be dependent on overcoming energetic barriers between local minima of similar energy on the quadruplex surface, rather than energetic differences between ligand conformations. Movement of the 3- and 6-side chains can be seen to be dependent mainly on the position of the charged terminal pyrrolidine group and the interaction this moiety makes with the spatially relevant DNA backbone. The side-chain length of compound **1a** is less than optimal, as neither side chain has the full potential to maximize its electrostatic and van der Waals (VDW) energy interactions with the corresponding loops. Compound **1b** is more favorable, the extra length in the side chains allowing more systematic sampling of the loop cavity, and the added flexibility of the side chains decreases the impact of variations in the loop structure on binding site and orientation during the MD simulations. However, with compounds **1c** and **1d**, the modeled structures at first sight appear to contrast with the data obtained from the biophysical experiment. In the model, the increased side-chain lengths of these two compounds would be expected to lead to a corresponding increase in quadruplex binding, yet this is not the conclusion from visual inspection of the MD trajectories.

Although qualitative observations on ligand−quadruplex interactions gave important insights into the behavior of the complex, attempts at quantitative correlations between the biophysical assay data and computationally derived ligand binding free energies were unsuccessful. This reflects the difficulties inherent in modeling DNA−ligand interactions using explicit solvent systems. Factors influencing this include the treatment of electrostatics and the relatively short time scale (1 ns) used for the MD simulations. Conformational sampling of ligand positions on the quadruplex surface is compromised by the short time scale nature of MD models, and the lack of an experimental DNA-ligand structure for the human intramolecular quadruplex complicates this issue. Additionally, it is likely that

the model neglects to give a complete representation of the balance between solvent exposure and DNA binding of the side chains. Increased side-chain flexibility may therefore lead not so much to tighter quadruplex binding but to increased solvent exposure, which is consistent with the experimental data.

The SAR of the 9-substituent suggests that it is required not just for its role in decreasing duplex intercalation but also as an important third moiety for interaction, for example, with the appropriate quadruplex loop. However, it is difficult to determine the extent to which quadruplex binding is dependent on electronic effects exerted on the acridine chromophore by the side chains. Changes in side-chain properties may thus have an impact on the acridine that is difficult to predict or model simply in terms of increases or decreases in binding due to VDW or electrostatic ligand−DNA interactions. This may be especially the case with the 9-anilinoacridines, in which the presence of the aniline group at the 9-position has been suggested to play an important electronic role in the protonation state (and hence physicochemical properties) of the acridine chromophore.[60−62]

In short, the structure−activity relationships of all three acridine substituents, taken together, are important for the overall effectiveness of a particular compound, and the modeling is consistent with the conclusion that it is difficult to break down the molecule and attempt to make individual modifications without altering the DNA−ligand contacts at other parts of the molecule. Targeting all three loops simultaneously is crucial, thereby increasing DNA−ligand contacts and facilitating stronger binding as well as selectivity. The modeling also highlights the key role of the quartet−acridine interaction, as was previously observed in the crystal structure of a disubstituted acridine with a dimeric quadruplex having diagonal loops.[63] Both the guanines and the chromophore of the ligands remained very stable over the course of the experiment, regardless of the side chains attached, although these are important for improving the selectivity and strength of binding, and variations in their structure are significant, although further work is required to accurately model the impact of side-chain modifications.

Cellular Effects. The cellular changes expected following exposure to telomere-targeting compounds are varied and complex, reflecting the interactions of telomeric proteins, DNA, and RNA involved in telomere maintenance. Targeting of telomeric DNA in particular is further complicated by issues of selectivity and specificity. However, the overall correlations between the quadruplex-affinity (FRET, SPR) and biochemical assay results (TRAP) suggest that these structure−activity relationships are derived primarily from the strength of the ligand−quadruplex DNA interaction, rather than more indirect effects that might modulate activity in a cell-based assay, such as interference with protein−quadruplex recognition or other macromolecular interactions. Above all, the efficacy of such compounds in the in vivo setting depends on their selectivity for quadruplex over duplex DNA, as well as their underlying drugability.

The specific inhibition of telomerase would be expected to result in an extended time lag associated with the gradual shortening of telomeres prior to the onset of replicative senescence. The MCF7 cell line has telomeres of average length 5−6 kb, and direct telomerase inhibition would thus be expected to take considerably longer (a loss of 4 kb at a rate of 100 bp per replication and 0.7 PD per day would occur after approximately 57 days). Compound **1b**, however, produces a pronounced antiproliferative effect within 1−2 weeks, at concentrations well below the IC_{50} value as determined in the SRB assay. Normal cell proliferation generally continued for a 1-week period before a major response was observed but then rapidly decreased following compound exposure, with a concomitant increase in observed senescence. The shape of the responses in terms of cell growth therefore suggests that the early change in growth rate observed was the initial cellular response to this type of damage: slowing population growth and increasing the number of cells entering senescence. Furthermore, the observed results are likely to be directly related to compound structure, as similar data have been reported for compound **1a**.[24,34] The shriveled morphology of the cells treated with **1b** may also be indicative of apoptotic cell death, and although the phenotype could not be accurately described in our hands, a shrunken cytoplasm and fragmented nuclei have been described as hallmarks of this process.[50] This reflects results such as those reported for the pentacyclic acridinium compound RHPS4, where onset of senescence has been described at higher concentration levels and apoptosis at lower ones,[25] or TMPyP4, which showed the same initial lack of effect but then elicited an apoptotic response in the following 2 weeks.[64] Further experiments are needed to investigate the possible induction of apoptosis under these experimental conditions.

In terms of senescence, the profile of increased senescence parallels the decrease in the number of population doublings over the first 1−2 weeks, perhaps indicating the accelerated senescence of the fraction of cells most affected by the compound. Moreover, the stabilization of the number of cells staining for senescence, as well as the population growth rate, after 3−4 weeks shows that there is a subpopulation that is particularly sensitive to exposure to the compound. This may be due to heterogeneity in telomere length (or less likely in the 3′-overhang), implying a subpopulation of cells with telomeres of shorter length than the population average. This is in accord with observations of telomere length using Southern blots, which show populations of cells with some having short telomeres.[34] Shorter telomeres would subsequently accelerate the onset of senescence,[10] which may be accelerated by the presence of the compounds, in agreement with the results of theoretical studies on the effects of telomerase inhibitors on population growth.[65,66]

The observed halt to cell growth may be a consequence of two separate but linked events, with senescence from telomere length reduction not being solely responsible for the decrease in population doublings It has been demonstrated that an alteration of telomere state, rather than simply telomere length, may be at least partially responsible for entry into replicative senescence,[67,68] and this altered state may rely heavily on the condition of the 3′-overhang, as it can be shown that much of this overhang is lost in senescent human cells.[6,7] In this hypothesis, a change in telomere state would signal initial entry into senescence while shortening of the overall telomere length results in diminished chromosome protection, triggering crisis.[11] This is of particular significance with respect to the biological data for compound **1b**, which showed significantly less short-term cytotoxicity (as measured in the SRB assay) in the human fibroblast cell line IMR90 than in the cancer cell line MCF7. This supports the postulate that telomeres and their associated capping mechanism are differently regulated in normal and cancer cells in a manner that is not simply dependent on the presence or absence of telomerase and therefore they represent a promising target for small-molecule intervention in their own right. There is increasing interest in nontelomeric quadruplexes as possible targets for selective drug action, and the promoter

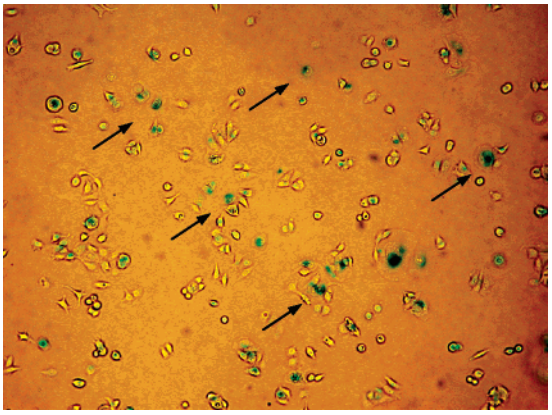

Figure 6. Representative picture of MCF7 cells following long-term (4-week) incubation with compound **1b** (1 μM) after staining for senescence-associated β-galactosidase (SA-β-Gal) activity (blue, arrows). Approximate magnification factor $\times$200.

regions of oncogenes such as *c-myc* have received special attention.[69] Such sites are within double-stranded DNA, contrasting with the uniquely single-stranded 3′-overhang telomeric DNA, and presumably are most accessible during transcription or replication. It has been calculated[68] that there are up to 350 000 potential quadruplex sites in the human genome (although it is likely that many cannot form stable quadruplexes[69]). Thus, the issue of selectivity for a particular quadruplex may be important. There is little data available to date, but one study has shown[70] that compound **1a** has a 5-fold selectivity for the human telomeric quadruplex compared to the *c-myc* one. This selectivity may be significantly higher in cells when the accessibility of these targets is taken into account. In a therapeutic setting, even a small effect that down-regulates the expression of oncogenes is beneficial.

Biological results for compound **1b**, which exhibits binding and telomerase inhibitory activity equivalent to those of **1a**, while suggesting an improved SAR, underline the short time scale of effects in the MCF7 breast cancer cell line and demonstrate a link between cell growth inhibition and the onset of senescence (Figure 6). Furthermore, these effects were observed at concentrations considerably below the reported short-term cytotoxicity (IC_{50}) value of the compound, and these studies showed that the compound is significantly more potent in this cancer cell line than in a normal somatic cell fibroblast line (IMR90). The inability of compound **1f** to produce cell growth arrest and senescence may be due to several factors; metabolism at the 9-substituent amide bond or reduced cellular uptake as a result of the additional charge on the pyrrolidine group at the 9-position are both possibilities. The calculated log *P* value for compounds **1a** and **1b** are respectively 1.4 and 1.9, whereas that for **1f** is -0.36. We conclude that potent telomerase inhibitory activity and quadruplex affinity are necessary though by themselves insufficient features for cellular activity. The extra charge at the 9-position in compound **1f** may well be one charge too many.

The biophysical and biochemical data overall suggest a number of structure−activity correlations for these trisubstituted acridines:

(i) With the 9-position substituents not having a cationic charge [i.e., compounds **1a**−**d**, with R = $N(CH_3)_2$], both quadruplex binding and telomerase inhibition are optimal with the shortest 3- and 6-side chains, i.e., with $n = 2$; extending the side chains by even one carbon atom beyond $n = 3$ has a highly deleterious effect on quadruplex binding and telomerase potency.

(ii) Protonation of the 9-position extended side chains in compounds **1e**−**j** results in elevated ΔT_m values and generally higher potency against telomerase.

(iii) Extending the 9-position substituent length does not have a major effect on either binding or potency. It is possible to counterbalance the adverse effects of extended 3,6- substituents with an extended substituent at the 9-position.

(iv) Selectivity for quadruplex over duplex DNA is correlated with both affinity and telomerase inhibition.

(v) Potency against telomerase and a high level of quadruplex affinity are necessary features though not sufficient by themselves for cellular activity. Compounds need to have appropriate cellular uptake and metabolic stability.

Of the compounds synthesized and evaluated in this study, only two, **1a** and **1b**, can be said to meet these criteria. An analogue of these has recently been chosen as a candidate for clinical studies in human cancer.

Materials and Methods

Fluorescence resonance energy transfer (FRET), PCR inhibition (TAQ), and telomeric repeat amplification protocol (TRAP) assays were carried out following previously published procedures,[39,52] while surface plasmon resonance (SPR) experiments were also conducted according to reported methods.[19,20]

FRET Assay. All oligonucleotides and their fluorescent conjugates (Eurogentec, Southampton, UK) were initially dissolved as a stock 50 μM solution in purified water; further dilutions were carried out in the relevant buffer. The labeled oligonucleotide F21T [5′-FAM-d(GGG[TTAGGG]$_3$)-TAMRA-3′; donor fluorophore FAM is 6-carboxyfluorescein; acceptor fluorophore TAMRA is 6-carboxytetramethylrhodamine] used as the FRET probe was diluted from stock solution to the correct concentration (400 nM) in a 50 mM potassium cacodylate buffer (pH 7.4) and then annealed by heating to 85 °C for 10 min, followed by cooling to room temperature in a heating block. Compounds were stored at −80 °C as 10 mM stock solutions in DMSO; final solutions were prepared using 10 mM HCl in the initial 1:10 dilution, after which 50 mM potassium cacodylate buffer (pH 7.4) was used in all subsequent steps. The 96-well plates (MJ Research, Waltham, MA) were prepared by aliquoting 50 μL of the annealed DNA into each well, followed by 50 μL of the compound solutions. Measurements were made in triplicate on a DNA Engine Opticon (MJ Research) with excitation at 450−495 nm and detection at 515−545 nm. Fluorescence readings were taken at intervals of 0.5 °C over the range 30−100 °C, with a constant temperature being maintained for 30 s prior to each reading to ensure a stable value. Final analysis of the data was carried out using the program Origin 7.0 (OriginLab Corp., Northampton, MA).

TAQ Assay. The procedure used was based on the internal control sequences that have been reported in the literature.[73] A master mix was prepared containing the TS forward primer (0.15 μg; 5′-AAT CCG TCG AGC AGA GTT-3′), NT reverse primer (0.5 μM; 5′-ATC GCT TCT CGG CCT TTT-3′), TSNT template (200 pM; 5′-AAT CCG TCG AGC AGA GTT AAA AGG CCG AGA AGC GAT-3′), $MgCl_2$ (1 mM), and equal amounts of dNTPs (20 μM), as well as *Taq* polymerase (1.25 U; RedHot, ABgene, Surrey, UK), in addition to the *Taq* reaction buffer (ABgene). All primers were obtained from Invitrogen (Paisley, UK) and had been HPLC-purified by the supplier. Compound solutions (prepared as before) were then pipetted into the reaction tubes, and the appropriate amount of master mix was added with mixing. Amplification was carried out using a two-step protocol with an initial denaturing step at 92 °C for 2 min, followed by 33 PCR cycles (92 °C for 30 s, 52 °C for 30 s, 72 °C for 45 s), and the 36 bp product was visualized on a 10% v/v polyacrylamide gel using SYBR Green I staining (Sigma).

TRAP Assay. Telomerase activity in the presence of the compounds was assessed using a modified version of standard published TRAP protocols.[39,73−75] Cell extract from exponentially

growing A2780 human ovarian carcinoma cells was used as the enzyme source and total protein upon extraction was quantitated using the standard Bradford assay method.[76] Briefly, the TRAP assay was carried out in two steps with an initial primer-elongation step and subsequent PCR amplification of the telomerase products to enable detection. In part 1, a master reaction mix was prepared containing the TS forward primer (0.1 μg; 5′-AAT CCG TCG AGC AGA GTT-3′), TRAP buffer [20 mM Tris-HCl (pH 8.3), 68 mM KCl, 1.5 mM $MgCl_2$, 1 mM EGTA, 0.05% v/v Tween-20], BSA (0.05 μg), and dNTPs (125 μM each). Compounds were prepared to 10 times final concentration (or vehicle controls) as described above, added to the PCR reaction tubes, and maintained at 0 °C. Simultaneously, the required amount of protein was thawed to 0 °C on ice and diluted in TRAP lysis buffer (pH 7.4, 0.5% CHAPS, 10 mM Tris-HCl, 1 mM $MgCl_2$, 1 mM EGTA, 5 mM β-mercaptoethanol, 10% glycerol) to the required concentration (500 μg/μL). The appropriate amount (2 μL) was then combined with the master mix on ice and aliquoted into the PCR tubes to give a final volume of 40 μL. The initial telomere elongation step was carried out for 10 min at 30 °C, followed by a protein heat inactivation step (4 min at 92 °C) and final maintenance of the mixture at 4 °C. Following heat inactivation of telomerase, 10 μL of a PCR reaction mix containing ACX primer (1 μM; 5′-GCG CGG $[CTTACC]_3$ CTA ACC-3′) and 2 U *Taq* polymerase (RedHot, ABgene, Surrey, UK) in TRAP reaction buffer was added to each tube to start the PCR protocol for part 2, with thermal cycling being carried out in three parts following an initial 2 min denaturing period at 92 °C (33 cycles of 92 °C for 30 s, 55 °C for 30 s, 72 °C for 45 s). The PCR-amplified reaction products were run out on a 10% v/v PAGE gel and visualized using SYBR green I (Sigma). $^{tel}EC_{50}$ values were calculated by quantitating the TRAP product using a gel scanner and GeneTools software (Syngene, Cambridge, UK). Measurements were made with respect to a negative control run using the equivalent TRAP−PCR conditions but with the protein extract either omitted or heat inactivated by incubation at 92 °C (20 min).

SPR Experiments. The Biosensor-SPR experiments were performed on BIAcore 2000 and 3000 optical biosensor systems using four-channel streptavidin-coated sensor chips (Biacore, Inc.) as previously described.[19,20] Briefly, streptavidin-coated sensor chips were preconditioned with three to five consecutive 1-mL injections of 1 M NaCl in 50 mM NaOH and washing with Hepes buffer at pH 7.4 [0.01 M Hepes, 0.20 M KCl, 3 mM EDTA, 0.005% (v/v) surfactant P20]. Conditioning was continued until the change in SPR signal was less than 1 RU/min. Immobilization of the DNA on the surface was carried out by noncovalent capture of biotinylated DNA sequences representative either of the human telomeric quadruplex (5′-biotin-d$[AG_3(TTAG_3)_3]$-3′) or a hairpin duplex DNA sequence (5′-biotin-CGAATTCG-CTCT-CGAATTCG-3′). Manual injection of 25 nM DNA in Hepes buffer (pH 7.4) at a flow rate of 2 μl/min was used in order to achieve long contact times with the surface and to better control the amount of DNA bound to the surface. Folding of the quadruplex DNA with respect to time under similar conditions to those used on the sensor chips was verified by a series of melting/cooling experiments using both CD and UV methods. All the binding study procedures were automated using cycles of sample injection and surface regeneration. To minimize possible unwanted mass transport effects, all SPR kinetics experiments were conducted at flow rates of 50−100 μL/min with low surface densities of immobilized DNA. For the steady-state analysis, flow rates were typically 10−30 μL/min. Global fitting of the association and dissociation curves was performed using the supplier's software (BIA Evaluation Software, Biacore, Inc.) and was done in a concentration range where the compounds bind significantly only to the strongest binding site.

Molecular Modeling. The crystal structure of the parallel 22mer telomeric G-quadruplex in potassium buffer (PDB ID 1KF1[18]) was used as the starting point for the computational work. Preparation and manipulation of the structure and initial building of the ligand−DNA complex prior to the molecular dynamics (MD) simulations was carried out using programs within the SYBYL 6.9 suite (Tripos, Inc., St. Louis, MO). Ligands were constructed in SYBYL, with charges and atom types applied using the MMFF94 method.[77,78] Stepwise minimizations using the MMFF94s force field[79] were subsequently carried out to a convergence of 0.02 kcal mol^{-1}/Å over 5000 steps using the Powell method[80] with a cutoff of 11 Å. This was followed by a conformational search on the ligand side chains (all rotatable bonds) using a genetic algorithm (GA) as implemented in SYBYL.[81−83] The 100 lowest energy conformers were generated using a search performed over 2×10^4 generations with a population of 1000 and a selective pressure of 1.5,[82] again with a cutoff of 11 Å and a dielectric constant of 80.

Following output from the conformational searches, quadruplex and ligand were brought into close proximity with the acridine chromophore parallel to the G-quartet (approximately distance 3.4 Å) and the acridine nitrogen placed above the central potassium channel. Ligand conformers with 3- or 6-side chains clashing with the DNA were then excluded, yielding generally between three and five structures for further work. Conformers chosen in this way were merged with the quadruplex and the aggregate (DNA plus ligand) and minimized in the same manner as has been described, with the DNA remaining fixed as a static set (convergence of 0.02 kcal mol^{-1}/Å, 5000 steps Powell minimization, cutoff 11 Å, dielectric constant of 4). Once merged, the structures were superimposed using the quadruplex as a template and the ligands separated from the complex to yield a molecular database containing the quadruplex and all the ligands docked in this manner. Subsequent preparation of the DNA−ligand complexes (with compounds **1a**−**d**), further minimizations, and molecular dynamics (MD) calculations were performed using the XLEAP, ANTECHAMBER, and SANDER modules of the AMBER7 package.[84,85]

All calculations were carried out in AMBER 7 using the Parm99 version of the Cornell et al. force field,[86] the TIP3P potential for waters,[87] the *parm99.dat* parameter set for the nucleic acids,[88] and GAFF atom types[85,89] for the ligand. Ligand charges were derived using the MMFF94 method[77] and defined in the ligand preparatory files as part of the new residue input. Periodic boundary conditions were applied, with the particle-mesh Ewald (PME) method[90] used to treat long-range electrostatic interactions. The solute was first solvated in a water-box, the dimensions of which extended to a distance at least 10 Å from any solute atom (total VDW box size approximately $61 \times 54 \times 50$ $Å^3$). Potassium counterions were subsequently added using XLEAP to attain overall system neutrality, with standard potassium parameters as applied in the Cornell et al. force field (VDW radius 2.658 Å).

Minimizations and MD runs were performed using SANDER, with the SHAKE algorithm enabled for hydrogen atoms in dynamics runs and a 1 fs time step with an 11 Å nonbonded cutoff. Overall equilibration of the system was carried out in successive steps, with initial equilibration of the system at constant volume followed by further rounds at constant pressure once the desired system temperature (300 K) had been reached. Following two primary rounds of solvent minimization, solute restraints were gradually reduced to 0.2 kcal mol^{-1}/Å over six 10 ps MD steps (100, 50, 25, 10, 5, 0.2), followed by 100 ps of unrestrained MD. The final geometry was then the starting point for the full 1 ns production run, with energy information and averages printed out every 250 steps, coordinates captured at 0.5 ps intervals, and the nonbonded list updated every 10 steps. Trajectories were examined visually using the VMD software package.[91] This allowed mapping of any large conformational changes to distinct time periods in the trajectory and the comparison with energy and rmsd values.

Sulforhodamine B (SRB) Growth Inhibition Aassay and Long-Term Cell Culture Experiments. The SRB assay was carried out in 96-well microtiter plates (Nunclon Surface, Nunc A/S, Denmark) according to published procedures.[30,47,48] Short-term cytotoxicity measurements were carried out in the human breast adenocarcinoma cell line MCF7 and in the human fibroblast cell line IMR90, both of which were obtained from the European Collection of Cell Cultures (Salisbury, UK).

Long-term experiments were carried out using the MCF7 cell line. Counting and media changes were carried out according to

standard procedures as has been reported,[24,30] with cells maintained in Dulbecco's modified Eagle's medium (DMEM; Invitrogen, Groningen, NL) supplemented with 10% v/v fetal calf serum (Life Technologies, Paisley, UK), 0.5 μg/mL hydrocortisone (Acros Chemicals, Loughborough, UK), 2 mM L-glutamine (Invitrogen), and a 1× solution of nonessential amino acids (Invitrogen) under a humidified 5% CO_2, 95% air atmosphere. Cell culture followed a regular weekly pattern based on the rate of growth and the cells reaching confluence, with counting, reseeding, and the first treatment on day 1 followed by reexposure at the same compound concentration on day 4. This protocol was maintained for 4−8 weeks, with analysis and staining experiments being carried out following the change of medium and transfer to a fresh flask on day 1.

Staining for Senescence-Associated β-Galactosidase (SA-β-Gal) Activity. Staining for SA-β-Gal activity was carried out according to the instructions of the supplier (Cell Signaling Technology, Inc., Beverly, MA). In brief, cells from long-term exposure studies were retrieved at the end of each week and seeded in 35 mm 6-well plates (Nunc A/S) at a density of 1×10^5 cells in 2 mL media and incubated overnight under standard conditions together with the appropriate concentration of the compound under investigation. After an approximately 24-h incubation period, the growth medium was removed, and the cells were washed, fixed, and stained using the supplied staining solution [400 mM citric acid/sodium phosphate (pH 6.0), 1.5 M NaCl, 20 mM $MgCl_2$, 5 mM potassium ferrocyanide, 5 mM potassium ferricyanide, 1 mg of X-gal (5-bromo-4-chloro-3-indolyl-β-D-galactopyranoside)], followed by incubation overnight at 37 °C (5% CO_2). Cells were examined by light microscope (mag. 200−800×) and counted the next day for the characteristic senescence-associated development of blue coloration.

Chemistry. Melting points (mp) were recorded on a Stuart Scientific SMP1 melting point apparatus and are uncorrected. IR spectra of solids were recorded using a Perkin-Elmer SPECTRUM 1000 FT-IR spectrometer. NMR spectra were recorded at 400 MHz (^{1}H) and 100 MHz (^{13}C) on a Bruker spectrometer in either $CDCl_3$ (Aldrich) or DMSO-d_6 (GOSS) or CD_3OD (GOSS) solutions using TMS as an internal standard or in the case of ^{13}C spectra the residual solvent peak of $CDCl_3$ and DMSO-d_6. Mass spectrometry services were provided by The School of Pharmacy (nominal and HRMS ESI, MALDI) and the EPSRC National Mass Spectrometry Service Centre (Chemistry Department, University of Wales, Swansea, Singleton Park, Swansea SA2 8PP, HRMS ESI). TLC analysis was carried out on silica gel (Merck 60F-254) with visualization at 254 and 366 nm. Treatment of an organic solution in the usual manner refers to stepwise drying with magnesium sulfate, filtration, and then evaporation of the filtrate in vacuo. Preparative flash chromatography was carried out with BDH silica gel (BDH 153325P). Reagents and chemicals unless indicated were purchased from Sigma-Aldrich. Solvents were purchased from BDH. *N*,*N*-Dimethylaminoaniline was generated by neutralization of the commercially available dihydrochloride salt**.** 6-Chlorohexanoyl chloride;[88] acridones **2**,[41] **3**,[19] and **7**;[19] 9-chloroacridines **11**[19] and **16**;[42] and acridines **1a**[19] and **22**[38] were prepared as reported. Details for the preparation of anilines **15a**−**c** and acridine **23** by treatment of 9-chloroacridine with aniline **15b** are presented in the Supporting Information, together with IR data on all compounds reported here. Analytical rpHPLC was performed with a Waters 600S Controller HPLC system connected to a Thermosep Products Spectra Series UV detector. HPLC method A1 had the following parameters: column, Hamilton C18; flow, 0.6 mL/min; gradient, 0−5 min, 20%-80% methanol in water containing 0.1% trifluoroacetic acid); detection, 290 nm. HPLC method B1 had the following parameters: column Phemonex Prodigy C18; flow, 1 mL/min; gradient, 0−27 min, 0%−46% acetonitrile in 30% acetonitrile in water containing 46 mM sodium octyl sulfonate with pH adjusted to 2.8 with phosphoric acid; detection 268 nm. Acridines **1b**−**j** were found to be >95% pure by applying HPLC method A1. The purity of **1b** and **1f**, which were submitted for cell biology studies, was also assessed with HPLC method B1. Details are presented in the Supporting Information. Analytical data for compound **1a** have been previously presented.[19]

3,6-Bis(chloroalkylamido)acridones (4−6). A suspension of **2** and acid chloride was heated at the specified temperature for the indicated time. The reaction suspension was allowed to cool to room temperature and placed in an ice bath, and ice-cold anhydrous diethyl ether was added. The solid produced was isolated by filtration and stirred in a 1:1 ice-cold mixture of aqueous sodium hydrogen carbonate and diethyl ether. This suspension was filtered, and the solid obtained was washed with ice-cold water and diethyl ether and dried in vacuo over phosphorus pentoxide to afford pure title product.

3,6-Bis[(pyrrolidin-1-yl)alkylamido]acridones (8−10). A solution of **4**, **5**, or **6** (stated amount) in pyrrolidine (stated volume) was heated under reflux for the specified time. The reaction solution was allowed to cool to room temperature and then poured into a stirred saturated aqueous sodium hydrogen carbonate solution (stated volume). Stirring was continued until a solid formed which was collected by suction filtration, washed with ice-cold diethyl ether and water, and then dried in vacuo over phosphorus pentoxide to afford title product.

3,6-Bis[(pyrrolidin-1-yl)alkylamido]-9-chloroacridines (12−14). A suspension of **8**, **9**, or **10** and phosphorus pentachloride and phosphorus oxychloride was heated under reflux with concomitant dissolution for the stated time. The reaction solution was allowed to cool to room temperature and then placed in an ice bath. Ice-cold anhydrous diethyl ether (stated volume) was then added to the cooled reaction solution. The resulting solid was isolated by suction filtration, washed thoroughly with anhydrous ice-cold diethyl ether, and then added portionwise to a stirred mixture of ice−aqueous ammonia solution (0.880)−chloroform in an ice-bath. Further ammonia solution was added to ensure the mixture remained alkaline. The chloroform layer was separated and the aqueous layer extracted with chloroform. The combined organic extracts were washed with brine and treated in the usual manner to give typically a dark brown residue that was triturated with ice-cold diethyl ether to afford a crude product which was submitted directly to the synthesis of trisubstituted acridines.

3,6-Bis(chloroalkylamido)-9-anilinoacridines (19−21). A suspension of **18** and the appropriate acid chloride, triethylamine, and toluene, if required, was microwaved at 150 °C for 5 min in fixed hold time mode. The resulting reaction mixtures were filtered to isolate the title compounds as solid products, which were then triturated with ether, dried, and immediately submitted to the next synthetic step.

3,6-Bis[(pyrrolidin-1-yl)alkylamido]-9-anilinoacridines (1). Method A (1a−j). Either *N*,*N*-dimethylaminoaniline or **15a**−**c** was added portionwise to a solution of the appropriate 9-chloroacridine **11**−**14** in MeOH (stated volume) and the resulting solution heated under reflux conditions for the stated time. The reaction solution was evaporated and the resulting red brown solid partitioned between chloroform and 20% aqueous ammonium hydroxide solution. The organic layer was separated and washed with brine and treated in the usual manner to give crude product as a red brown solid which was purified by flash chromatography eluting with the stated solvent mixture of dichloromethane and methanol with 10% v/v triethylamine. Fractions containing product were evaporated and partitioned again between chloroform and 20% dilute aqueous ammonium hydroxide solution. The organic layer was separated and the aqueous layer further extracted with chloroform. The combined organic extracts were washed with brine and then treated in the usual manner to give red brown solids, which were dried in a pistol in vacuo over phosphorus pentoxide to afford the pure title product.

Method B (1h−j). A solution of the 3,6-bis(chloroalkylamido)-9-anilinoacridine (**19**−**21**) in anhydrous pyrrolidine (1 mL) was stirred overnight at room temperature. LC/MS analysis at this point indicated reaction completion. The reaction solution was evaporated and the resulting crude product purified by flash chromatography eluting with 3:6:1 methanol/dichloromethane/triethylamine as described above for method A to give to pure title products.

3,6-Bis(4-chlorobutanamido)acridone (4). A brown suspension of **2** (5.019 g, 22 mmol) and 4-chlorobutyryl chloride (50 mL, 63 g, 450 mmol, 20 equiv) was heated at 80 °C overnight. The now yellow suspension was treated as described in the general methods to afford **4** (9.301 g, 96%) as a brown solid: mp 319 °C (dec); ^{1}H NMR (DMSO-d_6) δ 2.076 (m, 4H, J = 6.7 Hz), 2.571(t, 4H, J = 7.3 Hz), 3.734 (t, 4H, J = 6.5 Hz), 7.201 (dd, 2H, J = 1.9, 8.8 Hz), 8.089 (d, 2H, J = 8.8 Hz), 8.127 (d, 2H, J = 1.7 Hz), 10.370 (bs, 2H), 11.646 (bs, 1H); ^{13}C NMR (DMSO-d_6) δ 27.7, 33.5, 44.9, 48.5, 104.7, 113.2, 116.4, 126.8, 142.0, 143.1, 170.9, 175.0; HRMS (MALDI) m/z 434.1033 (MH^+, $C_{21}H_{22}N_3O_3$ requires 434.1033).

3,6-Bis(5-chloropentanamido)acridone (5). A brown suspension of **2** (1.002 g, 4 mmol) and 5-chlorovaleroyl chloride (6 mL, 7.2 g, 46 mmol, 12 equiv) was heated at 70 °C for 4 h. Treatment of the reaction mixture as described in the general methods gave **5** as a light brown solid (1.485 g, 72%): mp 337 °C (dec); ^{1}H NMR (DMSO-d_6) δ 1.768 (m, 8H), 2.427 (t, 4H, J = 6.8 Hz), 3.681 (t, 4H, J = 6.1 Hz), 7.191 (dd, 2H, J = 1.8, 8.8 Hz), 8.088 (d, 2H, J = 8.6 Hz), 8.129 (d, 2H, J = 1.4 Hz), 10.274 (bs, 2H), 11.614 (bs, 1H); ^{13}C NMR (DMSO-d_6) δ 22.3, 31.5, 35.6, 45.0, 104.6, 113.2, 116.3, 126.7, 142.0, 143.1, 171.6, 174.9; HRMS (MALDI) m/z 462.1346 (MH^+, $C_{23}H_{26}Cl_2N_3O_3$ requires 462.1346).

3,6-Bis(6-chlorohexanamido)acridone (6). A brown suspension of **2** (2.223 g, 0.01 mol) and 6-chlorohexanoyl chloride (16.39 g, 0.1 mol, 10 equiv) was heated at 70 °C for 5 h. Treatment of the reaction mixture as described in the general methods gave **6** as a brown solid (2.454 g, 51%): mp >350 °C (dec); ^{1}H NMR (DMSO-d_6) δ 1.448 (m, 4H), 1.654 (m, 4H), 1.761 (m, 4H), 2.397 (t, 4H, J = 7.3 Hz), 3.651 (t, 4H, J = 6.5 Hz), 7.191 (d, 2H, J = 8.8 Hz), 8.083 (d, 2H, J = 8.8 Hz), 8.134 (s, 2H), 10.256 (bs, 2H), 11.615 (bs, 1H); ^{13}C NMR (DMSO-d_6) δ 24.2, 25.9, 31.7, 36.3, 45.2, 104.6, 113.2, 116.3, 126.7, 142.0, 143.1, 171.8, 174.9; HRMS (MALDI) m/z 490.1659 (MH^+, $C_{25}H_{30}N_3O_3$ requires 490.1625).

3,6-Bis[4-(pyrrolidin-1-yl)butanamido]acridone (8). A solution of **4** (1.735 g, 4 mmol) in pyrrolidine (7 mL, 5.964 g, 84 mmol, 21 equiv) was heated under reflux overnight. The reaction solution was allowed to come to room temperature and cold saturated aqueous sodium hydrogen carbonate (30 mL) added with stirring. Stirring of the resulting oily mixture was continued until the point a brown solid collected. This solid was taken up into 10% hydrochloric acid, washed with dichloromethane, and then made basic with 5 N aqueous sodium hydroxide. The light brown solid formed was isolated by suction filtration and washed with cold ether and water. Yield **8** (1.564 g, 78%): mp 311 °C (dec); ^{1}H NMR (DMSO-d_6) δ 1.680−1.648 (m, 8H), 1.782 (m, 4H), 2.407−2.447 (m, 16H), 7.182 (dd, 2H, J = 1.9, 8.8 Hz), 8.074 (d, 2H, J = 8.8 Hz), 8.131 (d, 2H, J = 1.8 Hz), 10.275 (bs, 2H), 11.626 (bs, 1H); ^{13}C NMR (DMSO-d_6) δ 23.0, 24.2, 34.6, 53.4, 55.0, 104.6, 113.2, 116.3, 125.7, 142.1, 143.2, 172.0, 175.0; HRMS (ESI+) m/z 504.2969 (MH^+, $C_{29}H_{38}O_3N_5$ requires 504.2969).

3,6-Bis[5-(pyrrolidin-1-yl)pentanamido]acridone (9). The green solution of **5** (466 mg, 1 mmol) in pyrrolidine (5 mL, 4.26 g, 60 mmol, 60 equiv) was heated at reflux overnight. Treatment of reaction solution as described in the general methods gave **9** as a light brown solid (514 mg, 90%): mp >350 °C (dec); ^{1}H NMR (DMSO-d_6) δ 1.482 (m, 4H), 1.651 (m, 6H), 1.774 (m, 6H), 2.427 (m, 12H), 3.682 (t, 4H, J = 5.6 Hz), 7.192 (d, 2H, J = 8.4 Hz), 8.085 (d, 2H, J = 8.6 Hz), 8.129 (s, 2H), 10.291 (bs, 2H), 11.642 (bs, 1H); ^{13}C NMR (DMSO-d_6) δ 23.0, 23.1, 28.0, 36.4, 53.5, 55.3, 104.6, 113.2, 116.3, 126.7, 142.1, 143.2, 172.0, 175.0; HRMS (+ESI) m/z 532.3292 (MH^+, $C_{31}H_{42}N_5O_3$ requires 532.3282).

3,6-Bis[6-(pyrrolidin-1-yl)hexanamido]acridone (10). A solution of **6** (3.831 g, 8 mmol) in pyrrolidine (14 mL, 11.928 g, 168 mmol, 20 equiv) was heated under reflux for 15 h. The reaction solution was treated as described in the general methods to give **10** as a brown solid (3.295 g, 75%): mp >350 °C (dec); ^{1}H NMR (DMSO-d_6) δ 1.297−1.367 (m, 4H), 1.419−1.490 (m, 4H), 1.634 (m, 12H), 2.370 (m, 12H), 3.309 (t, 4H, J = 7.0 Hz), 7.186 (dd, 2H, J = 1.3 Hz, 8.8 Hz), 8.080 (d, 2H, J = 8.9 Hz), 8.132 (s, 2H), 10.239 (bs, 2H), 11.615 (bs, 1H); ^{13}C NMR (DMSO-d_6) δ 23.0, 25.0, 26.7, 28.2, 36.5, 53.5, 55.6, 104.6, 113.2, 116.3, 126.7, 142.0, 143.2, 172.0, 174.9; HRMS (+ESI) m/z 560.3595 (MH^+, $C_{33}H_{46}N_5O_3$ requires 560.3595).

3,6-Bis[4-(pyrrolidin-1-yl)butanamido]-9-chloroacridine (12). A suspension of **5** (3.029 g, 6 mmol) and phosphorus pentachloride (1.249 g, 6 mmol) in phosphorus oxychloride (20 mL) was refluxed for 2.5 h. The resulting solution was treated as described in the general methods to afford crude **12** as a brown solid (1.261 g, 40%).

3,6-Bis[5-(pyrrolidin-1-yl)pentanamido]-9-chloroacridine (13). A brown suspension of **9** (983 mg, 1.85 mmol) and phosphorus pentachloride (0.55 g, 2.6 mmol, 1.43 equiv) in phosphorus oxychloride (20 mL) was heated under reflux for 3 h. The reaction solution was treated as described in the general methods to afford crude **13** as a brown solid (600 mg, 59%).

3,6-Bis[6-(pyrrolidin-1-yl)hexanamido]-9-chloroacridine (14). A suspension of **10** (624 mg, 1.1 mmol) and phosphorus pentachloride (368 mg, 1.8 mmol, 1.6 equiv) in phosphorus oxychloride (15 mL) was heated under reflux for 3 h. The reaction solution was treated as described in the general methods to afford crude **14** as a brown solid (241 mg, 37%).

3,6-Diazido-9-{4′-[3″-(pyrrolidin-1-yl)propanamido]anilino}acridine (17). Aniline **15b** (62 mg, 0.2 mmol) was added to a solution of the diazido acridine **16** (6 mg, 0.2 mmol) in NMP (3 mL) followed by catalytic HCl (5 drops) and the resulting solution stirred at room temperature for 1 h, at which point TLC analysis indicated reaction completion. Ethyl acetate (15 mL) was added and the red solid produced isolated by filtration and washed with ethyl acetate and then diethyl ether to yield **14** as a red solid (86 mg, 87%): mp 200−205 °C; ^{1}H NMR (CD_3OD) δ 2.028 (m, 2H), 2.140 (m, 2H), 2.932 (t, 2H, J = 6.7 Hz), 3.132 (m, 2H), 3.537 (t, 2H, J = 6.5 Hz), 3.684 (m, 2H), 6.574 (d, 2H, J = 1.9 Hz), 6.608 (dd, 2H, J = 1.9, 9.3 Hz), 7.111 (d, 2H, J = 8.7 Hz), 7.605 (d, 2H, J = 8.7 Hz), 7.671 (d, 2H, J = 9.3 Hz); HRMS (+ESI) m/z 493.2220 (MH^+, $C_{26}H_{25}N_{10}O$ requires 493.2207).

3,6-Diamino-9-{4′-[3″-(pyrrolidin-1-yl)propanamido]anilino}acridine (18). A slurry of 10% Pd/C catalyst (3 mg) in ethyl acetate (0.5 mL) was added to a solution of **17** (25 mg, 0.0508 mmol) in methanol (5 mL) in a Parr hydrogenator flask and the reaction suspension shaken at 20 psi. H_2 for 1 h. At this point, LC/MS and TLC analysis indicated reaction completion. The mixture was filtered through Celite and the filtrate evaporated to give **18** as a red solid (15 mg, 67%): mp 205−210 °C; ^{1}H NMR (CD_3OD) δ 2.067 (m, 2H), 2.179 (m, 2H), 2.970 (t, 2H, J = 6.7 Hz), 3.171 (m, 2H), 3.576 (t, 2H, J = 6.5 Hz), 3.723 (m, 2H), 6.613 (d, 2H, J = 1.9 Hz), 6.647 (dd, 2H, J = 1.9, 9.4 Hz), 7.150 (d, J = 8.7 Hz), 7.644 (d, 2H, J = 8.7 Hz), 7.710 (d, J = 9.3 Hz); ^{13}C NMR (DMSO-d_6) δ 22.7, 32.0, 49.6, 52.9, 94.5, 105.5, 114.3, 119.9, 123.0, 127.2, 128.1, 128.8, 138.0, 142.9, 154.2, 167.6; HRMS (+ESI) m/z 441.2417 (MH^+, $C_{26}H_{29}N_6O$ requires 441.2397).

3,6-Bis(4-chlorobutanamido)-9-{4′-[3″-(pyrrolidin-1-yl)-propanamido]anilino}acridine (19). A suspension of **18** (30 mg, 0.068 mmol), 3-chloropropionyl chloride (2 mL), and triethylamine (37 μL, 27 mg, 0.27 mmol, 4 equiv) was microwaved and the resulting reaction mixture treated as described in the general methods to afford **19** as a red solid (35 mg, 79% yield): LC/MS (+ESI) m/z 649.27 (MH^+).

3,6-Bis(5-chloropentanamido)-9-{4′-[3″-(pyrrolidin-1-yl)-propanamido]anilino}acridine (20). A suspension of **18** (30 mg, 0.07 mmol), 5-chlorobutyryl chloride (2 mL), and triethylamine (37 μL, 27 mg, 0.27 mmol, 4 equiv) was microwaved and the resulting reaction mixture treated as described in the general methods to afford **20** as a red solid (37 mg, 80%): LC/MS (+ESI) m/z 677.30 (MH^+).

3,6-Bis(6-chlorohexanamido)-9-{4′-[3″-(pyrrolidin-1-yl)-propanamido]anilino}acridine (21). A suspension of **18** (25 mg, 0.06 mmol), 6-chlorohexanoyl chloride (48 mg, 0.29 mmol, 5 equiv), and triethylamine (32 μL, 23 mg, 0.23 mmol, 4 equiv) was microwaved and the resulting reaction mixture treated as described in the general methods to afford **21** as a red solid (24 mg, 59%): LC/MS (+ESI) m/z 705.25 (MH^+).

3,6-[4-(Pyrrolidin-1-yl)butanamido]-9-[4′-(*N*,*N*-dimethylamino)anilino]acridine (1b). By Method A. A dark red brown solution of *N*,*N*-dimethylaminoaniline (26 mg, 0.19 mmol, 1.1 equiv) and **12** (87 mg, 0.17 mmol) in anhydrous methanol (7 mL) was heated under reflux for 4 d. Product isolation and purification by flash chromatography eluting with a 3:6:1 mixture of methanol/dichloromethane/triethylamine gave **1b** as a red brown solid (13 mg, 13%): mp 112 °C (dec); ^{1}H NMR ($CDCl_3$, 3 mg/mL) δ 1.821 (m, 8H), 1.889 (m, 4H), 2.521 (m, 4H), 2.573 (m, 12H), 2.937 (s, 6H), 6.693 (d, 2H, J = 8.6 Hz), 6.903 (d, 2H, J = 7.8. Hz), 7.178 (bs, 2H), 7.825 (bs, 2H), 7.865 (bs, 2H), 10.229 (bs, 2H); HRMS (+ESI) m/z 622.3866 (MH^+, $C_{37}H_{48}N_7O_2$ requires 622.3864).

3,6-Bis[5-(pyrrolidin-1-yl)pentanamido]-9-[4′-(*N*,*N*-dimethylamino)anilino]acridine (1c). By Method A. An ice-cooled solution of *N*,*N*-dimethylaminoaniline dihydrochloride salt (170 mg, 0.8 mmol, 1.1 equiv) and triethylamine (125 μL, 91 mg, 0.9 mmol, 1.2 equiv) in anhydrous methanol (10 mL) was stirred for 15 minutes under nitrogen and then added slowly to an ice-cooled solution of **13** (408 mg, 0.74 mmol) in methanol (5 mL). The resulting solution was allowed to come to room temperature and then heated at reflux for 2 days under nitrogen. Product isolation and purification by flash chromatography eluting with 3:5:2 dichloromethane/methanol/triethylamine gave **1c** as a red brown solid (12 mg, 2%): mp 131−133 °C; ^{1}H NMR ($CDCl_3$, 1 mg/mL) δ 1.596 (m, 4H), 1.751 (bs, 12H), 2.487 (bs, 16H), 2.918 (s, 6H), 6.867 (d, 2H, J = 7.9 Hz), 6.662 (d, 2H, J = 8.5 Hz), 7.405 (bm, 2H), 7.807 (bm, 2H), 7.869 (bm, 2H), 9.363 (bs, 2H); HRMS (+ESI) m/z 650.4180 (MH^+, $C_{39}H_{52}N_7O_2$ requires 650.4177).

3,6-Bis[5-(pyrrolidin-1-yl)hexanamido]-9-[4′-(*N*,*N*-dimethylamino)anilino]acridine (1d). By Method A. An ice-cooled solution of *N*,*N*-dimethylaminoaniline dihydrochloride salt (99 mg, 0.47 mmol, 1.1 equiv) and triethylamine (0.2 mL, 1.43 mmol, 3.3 equiv) in anhydrous methanol (10 mL) was stirred for 15 minutes under nitrogen and then added slowly to a solution of **14** (248 mg, 0.43 mmol) in anhydrous methanol (10 mL). The resulting solution was allowed to come to room temperature and then heated at reflux for 2.5 d under nitrogen. Product isolation and purification by flash chromatography eluting with 3:6:1 methanol/dichloromethane/triethylamine gave **1d** as a red solid (19 mg, 12%): mp 159−161 °C; ^{1}H NMR ($CDCl_3$, 2 mg/mL) δ 1.379 (m, 4H), 1.589 (m, 4H), 1.688 (m, 4H), 1.805 (bs, 8H), 2.509 (m, 8H), 2.624 (bs, 8H), 2.935 (s, 6H), 6.627 (d, 2H, J = 8.2 Hz), 7.008 (d, 2H, J = 9.5 Hz), 7.519 (m, 2H), 7.833 (dd, 2H, J = 1.8, 7.5 Hz), 8.024 (bs, 2H), 9.977 (bs, 2H); HRMS (+ESI) m/z 678.4501 (MH^+, $C_{41}H_{56}N_7O_2$ requires 678.4490).

3,6-Bis[3-(pyrrolidin-1-yl)propionamido]-9-{4′-[2″-(pyrrolidin-1-yl)acetamido]anilino}acridine (1e). By Method A. A solution of **15a** (132 mg, 0.6 mmol) and **11** (300 mg, 0.6 mmol) in methanol (5 mL) was heated at 60 °C for 6 h. Product isolation and purification by flash chromatography eluting with 3:6:1 methanol/dichloromethane/triethylamine gave **1e** as a red brown solid (412 mg, 61%): mp 207−211 °C; ^{1}H NMR (**1e·4TFA**, DMSO-d_6) δ 1.832 (m, 2H), 1.886 (m, 6H), 2.028 (m, 6H), 2.814 (d, 2H, J = 4.645 Hz), 2.974 (t, 4H, J = 7.24 Hz), 3.086 (m, 6H), 3.493 (m, 6H), 3.572 (m, 6H), 7.336 (dd, 2H, J = 1.6, 9.5 Hz), 7.382 (d, 2H, J = 8.8 Hz), 7.719 (d, 2H, J = 8.9 Hz), 8.094 (d, 2H, J = 9.4 Hz), 8.508 (d, 2H, J = 1.6 Hz), 10.003 (s, 2H), 10.187 (s, 1H), 10.860 (s, 1H), 11.039 (s, 1H), 11.064 (s, 2H), 13.899 (s, 1H); HRMS (+ESI) m/z 677.3949 (MH^+, $C_{42}H_{35}N_8O_3$ requires 677.3922).

3,6-Bis[3-(pyrrolidin-1-yl)propionamido]-9-{4′-[3″-(pyrrolidin-1-yl)propanamido]anilino}acridine (1f). By Method A. A solution of **15b** (430 mg, 1.8 mmol, 3 equiv) and **11** (300 mg, 0.6 mmol) in methanol (50 mL) was heated under reflux for 15 h. Product isolation and purification by flash chromatography eluting with 3:6:1 methanol/dichloromethane/triethylamine gave **1f** as a red brown solid (290 mg, 60%): mp 147−149 °C; ^{1}H NMR (**1f·4TFA**, DMSO-d_6) δ 1.888 (m, 6H), 2.035 (m, 6H), 2.874 (t, 2H, J = 7.215 Hz), 2.969 (t, 4H, J = 7.3 Hz), 3.086 (m, 6H), 3.485 (m, 6H), 3.571 (m, 6H), 7.337 (m, 4H), 7.724 (d, 2H, J = 8.91 Hz), 8.087 (d, 2H, J = 9.5 Hz), 8.492 (d, 2H, J = 1.9 Hz), 9.932 (s, 1H), 10.063 (s, 2H), 10.519 (s, 1H), 11.032 (s, 1H), 11.066 (s, 2H), 13.861 (s, 1H); HRMS (+ESI) m/z 691.4078 ($C_{42}H_{35}N_8O_3$ requires 691.4078).

3,6-Bis[3-(pyrrolidin-1-yl)propionamido]-9-{4′-[3″-(pyrrolidin-1-yl)butanamido]anilino}acridine (1g). By Method A. A solution of **15c** (83 mg, 0.3 mmol, 3 equiv) in MeOH (5 mL) was added dropwise to a solution of **11** (50 mg, 0.1 mmol) in MeOH (5 mL) and the resulting solution heated at 40 °C for 5 h. Product isolation and then purification by recrystallization from MeOH/diethyl ether afforded **1g** as a red brown solid (39 mg, 55%): mp 168−170 °C; ^{1}H NMR (CD_3OD) δ 1.788−1.955 (m, 14H), 2.428 (t, 2H, J = 7.2 Hz), 2.674−2.774 (m, 10H), 2.962 (t, 4H, J = 7.1 Hz), 3.147 (t, 2H, J = 6.9 Hz), 3.341−3.472 (m, 6H), 6.684 (d, 2H, J = 8.8 Hz), 7.055(d, 2H, J = 8.7 Hz), 7.137 (dd, 2H, J = 1.9, 9.4 Hz), 7.961 (d, 2H, J = 9.4 Hz), 8.360 (d, 2H, J = 1.9 Hz); HRMS (+ESI) m/z 705.4206 (MH^+, $C_{41}H_{53}N_8O_3$ requires 705.4235).

3,6-Bis[4-(pyrrolidin-1-yl)butanamido]-9-{4′-[3″-(pyrrolidin-1-yl)propanamido]anilino}acridine (1h). By Method A. A solution of 9-chloroacridine **12** (534 mg, 1 mmol) and the aniline **15b** (725 mg, 3 mmol, 3 equiv) in methanol (20 mL) was heated under reflux for 4 days. Product isolation and purification by flash chromatography eluting with 3:6:1 methanol/dichloromethane/triethylamine gave **1d** as a red brown solid (82 mg, 11%).

By Method B. A solution of **19** (10 mg, 0.015 mmol) in anhydrous pyrrolidine (1 mL) was stirred overnight at room temperature. Product isolation and purification afforded **1h** as a red brown solid (7 mg, 60%): mp 176−179 °C; ^{1}H NMR (CD_3OD) δ 1.977−2.100 (m, 16H, J = 7.1 Hz), 2.530 (t, 2H, J = 6.51), 2.607 (t, 4H, J = 7.1 Hz), 2.78 (t, 2H, J = 7.1 Hz), 3.026 (m, 4H), 3.088 (t, 4H, J = 8.0 Hz), 3.180 (m, 8H), 7.171 (d, 2H, J = 8.8 Hz), 7.266 (dd, 2H, J = 1.9, 9.4 Hz), 7.646 (d, 2H, J = 8.9 Hz), 7.991 (d, 2H, J = 9.4 Hz), 8.405 (d, 2H, J = 1.8 Hz); HRMS (+ESI) m/z 719.4413 (MH^+, $C_{42}H_{55}N_8O_3$ requires 719.4391).

3,6-Bis[5-(pyrrolidin-1-yl)pentanamido]-9-{4′-[3″-(pyrrolidin-1-yl)propanamido]anilino}acridine (1i). By Method A. A solution of **15b** (7 mg, 0.2 mmol) and **13** (100 mg, 0.2 mmol) in methanol (10 mL) was heated under reflux for 4 days. Product isolation and purification by flash chromatography eluting with 3:6:1 methanol/dichloromethane/triethylamine afforded **1i** as a red brown solid (21 mg, 16%).

By Method B. A solution of **20** (10 mg, 0.02 mmol) in anhydrous pyrrolidine (1 mL) was stirred overnight at room temperature. Product isolation and purification afforded **1e** as a red brown solid (8 mg, 74%): mp 187−189 °C; ^{1}H NMR (CD_3OD) δ 1.762 (m, 8H), 1.955 (m, 8H), 1.984 (t, 4H, J = 7.1 Hz), 2.513 (t, 4H, J = 6.8 Hz), 2.668 (t, 2H, J = 7.2 Hz), 2.789 (m, 4H), 2.909 (t, 4H, J = 7.7 Hz), 3.001 (m, 8H), 3.217 (t, 2H, J = 7.2 Hz), 7.037 (d, 2H, J = 8.8 Hz), 7.213 (dd, 2H, J = 1.9, 9.3 Hz), 7.560 (d, 2H, J = 8.8 Hz), 7.950 (d, 2H, J = 9.3 Hz), 8.312 (d, 2H, J = 1.6 Hz); HRMS (+ESI) m/z 747.4702 (MH^+, $C_{44}H_{59}N_8O_3$ requires 747.4705).

3,6-Bis[4-(pyrrolidin-1-yl)hexanamido]-9-{4′-[3″-(pyrrolidin-1-yl)propanamido]anilino}acridine (1j). By Method A. A solution of **15b** (128 mg, 0.6 mmol, 1.2 equiv) and **14** (284 mg, 0.5 mmol) in methanol was heated under reflux for 2.5 d. Product isolation and purification as described in the general methods afforded **1f** as a red brown solid (44 mg, 12%).

By Method B. A solution of **21** (12 mg, 0.017 mmol) in anhydrous pyrrolidine (1 mL) was stirred overnight at room temperature. Product isolation and purification by flash chromatography eluting with 3:6:1 methanol/dichloromethane/triethylamine afforded **1**f as a red brown solid (5 mg, 38%): mp 134−136 °C; ^{1}H NMR (CD_3OD) δ 1.471 (quintet, 4H, J = 7.6 Hz), 1.695−1.816 (m, 8H), 1.910 (m, 4H), 1.987 (m, 8H), 2.488 (t, 4H, J = 7.4), 2.691 (t, 2H, J = 7.2 Hz), 2.833 (m, 4H), 2.969 (t, 4H, J = 8.1 Hz), 3.048 (t, 2H, J = 7.0 Hz), 3.100 (m, 8H), 7.068 (d, 2H, J = 8.8 Hz), 7.230 (dd, 2H, J = 2.0, 9.3 Hz), 7.582 (d, 2H, J = 8.8 Hz), 7.953 (d, 2H, J = 9.3 Hz), 8.327 (d, 2H, J = 1.8 Hz); HRMS (+ESI) m/z 775.5029 (MH^+, $C_{46}H_{63}N_8O_3$ requires 775.5018).

Acknowledgment. This work has been supported by Cancer Research UK (Program and Project Grants to S. N. and a Research Studentship to C.M.S.), by grants from the Association for International Cancer Research and Antisoma Ltd (to S.N.), and by NIH Grant No. GM61587 (to W.D.W.). We are grateful to various colleagues for advice and discussions, especially Prof. Lloyd Kelland (Antisoma).

Supporting Information Available: Experimental procedures and spectral data for compounds **15a**−**c** and **23**, rpHPLC purity data, and SPR sensorgrams for compound **1b**. This material is available free of charge via the Internet at http://pubs.acs.org.

References

(1) Blackburn, E. H. Telomere states and cell fates. *Nature* **2000**, *408*, 53−56.
(2) Blackburn, E. H. Switching and signaling at the telomere. *Cell* **2001**, *106*, 661−673.
(3) Karlseder, J.; Smogorzewska, A.; de Lange, T. Senescence induced by altered telomere state, not telomere loss. *Science* **2002**, *295*, 2446−2449.
(4) Liu, D.; O'Connor, M. S.; Qin, J.; Songyang, Z. Telosome−A mammalian telomere associated complex formed by multiple telomeric proteins. *J. Biol. Chem.* **2004**, *279*, 51338−51342.
(5) (a) Smogorzewska, A.; de Lange, T. Regulation of telomerase by telomeric proteins. *Annu. Rev. Biochem.* **2004**, *73*, 177−208. (b) de Lange, T. Shelterin: The protein complex that shapes and safeguards human telomeres. *Genes Dev.* **2005**, *19*, 2100−2110.
(6) Li, G. Z.; Eller, M. S.; Firoozabadi, R.; Gilchrest, B. A. Evidence that exposure of the telomere 3′ overhang sequence induces senescence. *Proc. Natl. Acad. Sci. U.S.A.* **2003**, *100*, 527−531.
(7) Stewart, S. A.; Ben Porath, I.; Carey, V. J.; O'Connor, B. F.; Hahn, W. C.; Weinberg, R. A. Erosion of the telomeric single-strand overhang at replicative senescence. *Nat. Genet.* **2003**, *33*, 492−496.
(8) Steinert, S.; Shay, J. W.; Wright, W. E. Transient expression of human telomerase extends the life span of normal human fibroblasts. *Biochem. Biophys. Res. Commun.* **2000**, *273*, 1095−1098.
(9) Counter, C. M.; Avilion, A. A.; LeFeuvre, C. E.; Stewart, N. G.; Greider, C. W.; Harley, C. B.; Bacchetti, S. Telomere shortening associated with chromosome instability is arrested in immortal cells which express telomerase activity. *EMBO J.* **1992**, *11*, 1921−1929.
(10) Hemann, M. T.; Strong, M. A.; Hao, L. Y.; Greider, C. W. The shortest telomere, not average telomere length, is critical for cell viability and chromosome stability. *Cell* **2001**, *107*, 67−77.
(11) Masutomi, K.; Yu, E. Y.; Khurts, S.; Ben-Porath, I.; Currier, J. L.; Metz, G. B.; Brooks, M. W.; Kaneko, S.; Murakami, S.; DeCaprio, J. A.; Weinberg, R. A.; Stewart, S. A.; Hahn, W. C. Telomerase maintains telomere structure in normal human cells. *Cell* **2003**, *114*, 241−253.
(12) Counter, C. M.; Hirte, H. W.; Bacchetti, S.; Harley, C. B. Telomerase activity in human ovarian carcinoma. *Proc. Natl. Acad. Sci. U.S.A.* **1994**, *91*, 2900−2904.
(13) Kim, N. W.; Piatyszek, M. A.; Prowse, K. R.; Harley, C. B.; West, M. D.; Ho, P. L.; Corviello, G. M.; Wright, W. E.; Weinrich, S. L.; Shay, J. W. Specific association of human telomerase activity with immortal cells and cancer. *Science* **1994**, *266*, 2011−2015.
(14) Shay, J. W.; Bacchetti, S. A survey of telomerase activity in human cancer. *Eur. J Cancer* **1997**, *33*, 787−791.
(15) Hahn, W. C.; Counter, C. M.; Lundberg, A. S.; Beijersbergen, R. L.; Brooks, M. W.; Weinberg, R. A. Creation of human tumour cells with defined genetic elements. *Nature* **1999**, *400*, 464−468.
(16) Neidle, S.; Parkinson, G. Telomere maintenance as a target for anticancer drug discovery. *Nat. Rev. Drug Discovery* **2002**, *1*, 383−393.
(17) Neidle, S.; Parkinson, G. N. The structure of telomeric DNA. *Curr. Opin. Struct. Biol.* **2003**, *13*, 275−283.
(18) Parkinson, G. N.; Lee, M. P.; Neidle, S. Crystal structure of parallel quadruplexes from human telomeric DNA. *Nature* **2002**, *417*, 876−880.
(19) Harrison, R. J.; Cuesta, J.; Chessari, G.; Read, M. A.; Basra, S. K.; Reszka, A. P.; Morrell, J.; Gowan, S. M.; Incles, C. M.; Tanious, F. A.; Wilson, W. D.; Kelland, L. R.; Neidle, S. Trisubstituted acridine derivatives as potent and selective telomerase inhibitors. *J. Med. Chem.* **2003**, *46*, 4463−4476.
(20) Read, M.; Harrison, R. J.; Romagnoli, B.; Tanious, F. A.; Gowan, S. M.; Reszka, A. P.; Wilson, W. D.; Kelland, L. R.; Neidle, S. Structure-based design of selective and potent G quadruplex-mediated telomerase inhibitors. *Proc. Natl. Acad. Sci. U.S.A.* **2001**, *98*, 4844−4849.
(21) Gowan, S. M.; Heald, R.; Stevens, M. F.; Kelland, L. R. Potent inhibition of telomerase by small-molecule pentacyclic acridines capable of interacting with G-quadruplexes. *Mol. Pharm.* **2001**, *60*, 981−988.
(22) Alberti, P.; Schmitt, P.; Nguyen, C. H.; Rivalle, C.; Hoarau, M.; Grierson, D. S.; Mergny, J. L. Benzoindoloquinolines interact with DNA tetraplexes and inhibit telomerase. *Bioorg. Med. Chem. Lett.* **2002**, *12*, 1071−1074.
(23) Kim, M. Y.; Vankayalapati, H.; Shin-Ya, K.; Wierzba, K.; Hurley, L. H. Telomestatin, a potent telomerase inhibitor that interacts quite specifically with the human telomeric intramolecular G-quadruplex. *J. Am. Chem. Soc.* **2002**, *124*, 2098−2099.
(24) Gowan, S. M.; Harrison, R. J.; Patterson, L.; Valenti, M.; Read, M. A.; Neidle, S.; Kelland, L. R. A G-quadruplex-interactive potent small-molecule inhibitor of telomerase exhibiting in vitro and in vivo antitumor activity. *Mol. Pharm.* **2002**, *61*, 1154−1162.
(25) (a) Leonetti, C.; Amodei, S.; D'Angelo, C.; Rizzo, A.; Benassi, B.; Antonelli, A.; Elli, R.; Stevens, M. F. G.; D'Incalci, M.; Zupi, G.; Biroccio, A. Biological Activity of the G-quadruplex ligand RHPS4 (3,11-difluoro-6,8,13-trimethyl-8*H*-quino[4,3,2-*kl*] acridinium methosulfate) is associated with telomere capping alteration. *Mol. Pharm.* **2004**, *66*, 1138−1146. (b) Granotier, C.; Pennarun, G.; Riou, L.; Hoffschir, F.; Gauthier, L. R.; de Chian, A.; Gomez, D.; Mandine, E.; Riou, J.-F.; Mergny, J.-L.; Mailliet, P.; Dutrillaux, B.; Boussin, F. D. Preferential binding of a G-quadruplex ligand to human chromosome ends. *Nucleic Acids Res.* **2005**, *33*, 4182−4190. (c) Pennarun, G.; Granotier, C.; Gauthier, L. R.; Gomez, D.; Hoffschir, F.; Mandine, E.; Riou, J.-F.; Mergny, J.-L.; Mailliet, P.; Boussin, F. Apoptosis related to telomere instability and cell cycle alterations in human giolma cells treated by new highly selective G-quadruplex ligands. *Oncogene* **2005**, *24*, 2917−2928.
(26) Gomez, D.; Paterski, R.; Lemarteleur, T.; Shin-ya, K.; Mergny, J.-L.; Riou, J.-F. Interaction of telomestatin with the telomeric single-strand overhang. *J. Biol. Chem.* **2004**, *279*, 41487−41494.
(27) Lei, M.; Podell, E. R.; Cech, T. R. Structure of human POT1 bound to telomeric single-stranded DNA provides a model for chromosome end-protection. *Nature Struct. Mol. Biol.* **2004**, *11*, 1223−1229.
(28) Colgin, L. M.; Baran, K.; Baumann, P.; Cech, T. R.; Reddel, R. R. Human POT1 facilitates telomere elongation by telomerase. *Curr. Biol.* **2003**, *13*, 942−946.
(29) (a) Baumann, P.; Cech, T. R. Pot1, the putative telomere end-binding protein in fission yeast and humans. *Science* **2001**, *292*, 1171−1175. (b) Zaug, A. J.; Podell, E. R.; Cech, T. R. Human POT1 disrupts telomeric G-quadruplexes allowing telomerase extension in vitro. *Proc. Natl. Acad. Sci. U.S.A.* **2005**, *102*, 10864−10869. (c) Paeschek, K.; Simonsson, T.; Postberg, J.; Rhodes, D.; Lipps, H. J. Telomere end-binding proteins control the formation of G-quadruplex DNA structures in vivo. *Nature Struct. Mol. Biol.* **2005**, in press.
(30) Incles, C. M.; Schultes, C. M.; Kempski, H.; Koehler, H.; Kelland, L. R.; Neidle, S. A G-quadruplex telomere targeting agent produces p16-associated senescence and chromosomal fusions in human prostate cancer cells. *Mol. Cancer Ther.* **2004**, *3*, 1201−1206.
(31) Sun, H.; Karow, J. K.; Hickson, I. D.; Maizels, N. The Bloom's syndrome helicase unwinds G4 DNA. *J. Biol. Chem.* **1998**, *273*, 27587−27592.
(32) Opresko, P. L.; Von Kobbe, C.; Laine, J. P.; Harrigan, J.; Hickson, I. D.; Bohr, V. A. Telomere-binding protein TRF2 binds to and stimulates the Werner and Bloom syndrome helicases. *J. Biol. Chem.* **2002**, *277*, 41110−41119.
(33) Li, J. L.; Harrison, R. J.; Reszka, A. P.; Brosh, R. M., Jr.; Bohr, V. A.; Neidle, S.; Hickson, I. D. Inhibition of the Bloom's and Werner's syndrome helicases by G-quadruplex interacting ligands. *Biochemistry* **2001**, *40*, 15194−15202.
(34) Burger, A. M.; Dai, F.; Schultes, C. M.; Reszka, A. P.; Moore, M. J.; Double, J. A.; Neidle, S. The G-quadruplex-interactive molecule BRACO-19 inhibits tumor growth, consistent with telomere targeting and interference with telomerase function. *Cancer Res.* **2005**, *65*, 1489−1496.
(35) Chen, Z.; Corey, D. R. Telomerase inhibitors: A new option for chemotherapy. *Adv. Cancer Res.* **2003**, *87*, 31−58.
(36) Shay, J. W.; Wright, W. E. Telomerase: A target for cancer therapeutics. *Cancer Cell* **2002**, *2*, 257−265.
(37) (a) Mergny, J. L.; Riou, J. F.; Mailliet, P.; Teulade-Fichou, M. P.; Gilson, E. Natural and pharmacological regulation of telomerase. *Nucleic Acids Res.* **2002**, *30*, 839−865. (b) Kelland, L. R. Overcoming the immortality of tumour cells by telomere and telomerase based cancer therapeutics−Current status and future prospects. *Eur. J. Cancer* **2005**, *41*, 971−979.
(38) Harrison, R. J.; Gowan, S. M.; Kelland, L. R.; Neidle, S. Human telomerase inhibition by substituted acridine derivatives. *Bioorg. Med. Chem. Lett.* **1999**, *9*, 2463−2468.

(39) Schultes, C. M.; Guyen, B.; Cuesta, J.; Neidle, S. Synthesis, biophysical and biological evaluation of 3,6-bis-amidoacridines with extended 9-anilino substituents as potent G-quadruplex-binding telomerase inhibitors. *Bioorg. Med. Chem. Lett.* **2004**, *14*, 4347−4351.

(40) Harrison, R. J.; Reszka, A. P.; Haider, S. M.; Romagnoli, B.; Morrell, J.; Read, M. A.; Gowan, S. M.; Incles, C. M.; Kelland, L. R.; Neidle, S. Evaluation of disubstituted acridone derivatives as telomerase inhibitors: The importance of G-quadruplex binding. *Bioorg. Med. Chem. Lett.* **2004**, *14*, 5845−5849.

(41) Matsumura, K. The synthesis of certain acridine compounds. *J. Am. Chem. Soc.* **1929**, *51*, 816−820.

(42) Gamage, S. A.; Tepsiri, N.; Wilairat, P.; Wojcik, S. J.; Figgitt, D. P.; Ralph, R. K.; Denny, W. A. Synthesis and in vitro evaluation of 9-anilino-3,6-diaminoacridines active against a multidrug-resistant strain of the malaria parasite Plasmodium falciparum. *J. Med. Chem.* **1994**, *37*, 1486-1494.

(43) Spackova, N.; Berger, I.; Sponer, J. Nanosecond molecular dynamics simulations of parallel and antiparallel guanine quadruplex DNA molecules. *J. Am. Chem. Soc.* **1999**, *121*, 5519−5534.

(44) Spackova, N.; Berger, I.; Sponer, J. Structural dynamics and cation interactions of DNA quadruplex molecules containing mixed guanine/cytosine quartets revealed by large-scale MD simulations. *J. Am. Chem. Soc.* **2001**, *123*, 3295−3307.

(45) Fadrna, E.; Spackova, N.; Stefl, R.; Koca, J.; Cheatham, T. E.; Sponer, J. Molecular dynamics simulations of guanine quadruplex loops: Advances and force field limitations. *Biophys. J.* **2004**, *87*, 227−242.

(46) Hazel, P.; Huppert, J.; Balasubramanian, S.; Neidle, S. Loop-length-dependent folding of G-quadruplexes. *J. Am. Chem. Soc.* **2004**, *126*, 16405−16415.

(47) Skehan, P.; Storeng, R.; Scudiero, D.; Monks, A.; McMahon, J.; Vistica, D.; Warren, J. T.; Bokesch, H.; Kenney, S.; Boyd, M. R. New colorimetric cytotoxicity assay for anti-cancer-drug screening. *J. Natl. Cancer Inst.* **1990**, *82*, 1107−1112.

(48) Papazisis, K. T.; Geromichalos, G. D.; Dimitriadis, K. A.; Kortsaris, A. H. Optimization of the sulforhodamine B colorimetric assay. *J. Immunol. Methods* **1997**, *208*, 151−158.

(49) Hwang, E. S. Replicative senescence and senescence-like state induced in cancer-derived cells. *Mech. Aging Dev.* **2002**, *123*, 1681−1694.

(50) Roninson, I. B. Tumor senescence as a determinant of drug response in vivo. *Drug Resistance Updates* **2002**, *5*, 204−208.

(51) Roninson, I. B.; Broude, E. V.; Chang, B. D. If not apoptosis, then what? Treatment-induced senescence and mitotic catastrophe in tumor cells. *Drug Resistance Updates* **2001**, *4*, 303−313.

(52) Guyen, B.; Schultes, C. M.; Hazel, P.; Mann, J.; Neidle, S. Synthesis and evaluation of analogues of 10H-indolo[3,2-b]quinoline as G-quadruplex stabilising ligands and potential inhibitors of the enzyme telomerase. *Org. Biomol. Chem.* **2004**, *2*, 981−988.

(53) Mergny, J. L.; Lacroix, L.; Teulade-Fichou, M. P.; Hounsou, C.; Guittat, L.; Hoarau, M.; Arimondo, P. B.; Vigneron, J. P.; Lehn, J. M.; Riou, J. F.; Garestier, T.; Helene, C. Telomerase inhibitors based on quadruplex ligands selected by a fluorescence assay. *Proc. Natl. Acad. Sci. U.S.A.* **2001**, *98*, 3062−3067.

(54) Koeppel, F.; Riou, J. F.; Laoui, A.; Mailliet, P.; Arimondo, P. B.; Labit, D.; Petitgenet, O.; Helene, C.; Mergny, J. L. Ethidium derivatives bind to G-quartets, inhibit telomerase and act as fluorescent probes for quadruplexes. *Nucleic Acids Res.* **2001**, *29*, 1087−1096.

(55) Risitano, A.; Fox, K. R. Influence of loop size on the stability of intramolecular DNA quadruplexes. *Nucleic Acids Res.* **2004**, *32*, 2598−2606.

(56) Stefl, R.; Cheatham, T. E.; Spackova, N.; Fadrna, E.; Berger, I.; Koca, J.; Sponer, J. Formation pathways of a guanine-quadruplex DNA revealed by molecular dynamics and thermodynamic analysis of the substates. *Biophys. J.* **2003**, *85*, 1787−1804.

(57) Williamson, J. R.; Raghuraman, M. K.; Cech, T. R. Monovalent cation-induced structure of telomeric DNA: The G-quartet model. *Cell* **1989**, *59*, 871−880.

(58) Schultze, P.; Hud, N. V.; Smith, F. W.; Feigon, J. The effect of sodium, potassium and ammonium ions on the conformation of the dimeric quadruplex formed by the Oxytricha nova telomere repeat oligonucleotide d(G(4)T(4)G(4)). *Nucleic Acids Res.* **1999**, *27*, 3018−3028.

(59) Gavathiotis, E.; Heald, R. A.; Stevens, M. F.; Searle, M. S. Recognition and Stabilization of quadruplex DNA by a potent new telomerase inhibitor: NMR studies of the 2:1 complex of a pentacyclic methylacridinium cation with d(TTAGGGT)(4). *Angew. Chem. Int. Ed.* **2001**, *40*, 4749−4751.

(60) Denny, W. A.; Cain, B. F.; Atwell, G. J.; Hansch, C.; Panthananickal, A.; Leo, A. Potential antitumor agents. 36. Quantitative relationships between experimental antitumor activity, toxicity, and structure for the general class of 9-anilinoacridine antitumor agents. *J. Med. Chem.* **1982**, *25*, 276−315.

(61) Denny, W. A.; Atwell, G. J.; Baguley, B. C. Potential antitumor agents. 39. Anilino ring geometry of amsacrine and derivatives: Relationship to DNA binding and antitumor activity. *J. Med. Chem.* **1983**, *26*, 1625−1630.

(62) Gao, H.; Denny, W. A.; Garg, R.; Hansch, C. Quantitative structure−activity relationships (QSAR) for 9-anilinoacridines: A comparative analysis. *Chemico-Biol. Interactions* **1998**, *116*, 157−180.

(63) Haider, S. M.; Parkinson, G. N.; Neidle, S. Structure of a G-quadruplex-ligand complex. *J. Mol. Biol.* **2003**, *326*. 117−25.

(64) Shammas, M. A.; Shmookler Reis, R. J.; Akiyama, M.; Koley, H.; Chauhan, D.; Hideshima, T.; Goyal, R. K.; Hurley, L. H.; Anderson, K. C.; Munshi, N. C. Telomerase inhibition and cell growth arrest by G-quadruplex interactive agent in multiple myeloma. *Mol. Cancer Ther.* **2003**, *2*, 825−833.

(65) Sidorov, I. A.; Hirsch, K. S.; Harley, C. B.; Dimitrov, D. S. Cancer cell dynamics in the presence of telomerase inhibitors: Analysis of in vitro data. *J. Theor. Biol.* **2002**, *219*, 225−233.

(66) Sidorov, I. A.; Hirsch, K. S.; Harley, C. B.; Dimitrov, D. S. Cancer treatment by telomerase inhibitors: Predictions by a kinetic model. *Mathematical Biosciences* **2003**, *181*, 209−221.

(67) Stewart, S. A.; Hahn, W. C.; O'Connor, B. F.; Banner, E. N.; Lundberg, A. S.; Modha, P.; Mizuno, H.; Brooks, M. W.; Fleming, M.; Zimonjic, D. B.; Popescu, N. C.; Weinberg, R. A. Telomerase contributes to tumorigenesis by a telomere length-independent mechanism. *Proc. Natl. Acad. Sci. U.S.A.* **2002**, *99*, 12606−12611.

(68) Zou, Y.; Sfeir, A.; Gryaznov, S. M.; Shay, J. W.; Wright, W. E. Does a sentinel or a subset of short telomeres determine replicative senescence? *Mol. Biol. Cell* **2004**, *15*, 3709−3718.

(69) Siddiqui-Jain, A.; Grand, C. L.; Bearss, D. J.; Hurley, L. H. Direct evidence for a G-quadruplex in a promoter region and its targeting with a small molecule to repress c-MYC transcription. *Proc. Natl. Acad. Sci. U.S.A.* **2002**, *99*, 11593−11598.

(70) (a) Huppert, J.; Balasubramanian, S. Prevalence of quadruplexes in the human genome. *Nucleic Acids Res.* **2005**, *33*, 2908−2916. (b) Todd, A. K.; Johnston, M.; Neidle, S. Highly prevalent putative quadruplex sequence motifs in human DNA. *Nucleic Acids Res.* **2005**, *33*, 2901−2907.

(71) Rankin, S.; Reszka, A. P.; Huppert, J.; Zloh, M.; Parkinson, G. N.; Todd, A. K.; Ladame, S. L.; Balasubramanian, S.; Neidle, S. Putative DNA quadruplex formation within the human c-kit oncogene. *J. Am. Chem. Soc.* **2005**, *127*, 10584−10589.

(72) Lemarteleur, T.; Gomez, D.; Paterski, R.; Mandine, E.; Mailliet, P.; Riou, J.-F. Stabilization of the c-myc gene promoter quadruplex by specific ligands' inhibitors of telomerase. *Biochem. Biophys. Res. Commun.* **2004**, *323*, 802−888.

(73) Kim, N. W.; Wu, F. Advances in quantification and characterization of telomerase activity by the telomeric repeat amplification protocol (TRAP). *Nucleic Acids Res.* **1997**, *25*, 2595−2597.

(74) Burger, A. M. Standard TRAP Assay. In *Telomeres and Telomerase: Methods and Protocols*; Double, J. A., Thompson, M. J., Eds.; Humana Press Inc.: Totowa, NJ, 2002; pp 109−124.

(75) Gomez, D.; Mergny, J. L.; Riou, J. F. Detection of telomerase inhibitors based on G-quadruplex ligands by a modified telomeric repeat amplification protocol assay. *Cancer Res.* **2002**, *62*, 3365−3368.

(76) Bradford, M. M. A rapid and sensitive method for the quantitation of microgram quantities of protein utilizing the principle of protein-dye binding. *Anal. Biochem.* **1976**, *72*, 248−254.

(77) Halgren, T. A. Merck Molecular Force Field. I. Basis, form, scope, parametrization and performance of MMFF94. *J. Comput. Chem.* **1996**, *17*, 490−519.

(78) Halgren, T. A. Merck Molecular Force Field. VII. Characterization of MMFF94, MMFF94s, and other widely available force fields for conformational energies and for intermolecular-interaction energies and geometries. *J. Comput. Chem.* **1999**, *20*, 730−748.

(79) Halgren, T. A. Merck Molecular Force Field. VI. MMFF94s option for energy minimization studies. *J. Comput. Chem.* **1999**, *20*, 720−729.

(80) Powell, M. J. D. Restart procedures for the conjugate gradient method. *Math. Programming* **1977**, *12*, 241−254.

(81) Judson, R. S.; Jaeger, E. P.; Treasurywala, A. M.; Peterson, M. L. Conformational searching methods for small molecules 2. Genetic algorithm approach. *J. Comput. Chem.* **1993**, *14*, 1407−1414.

(82) McGarrah, D. B.; Judson, R. S. Analysis of the genetic algorithm method of molecular conformation determination. *J. Comput. Chem.* **1993**, *14*, 1385−1395.

(83) Clark, M.; Cramer, R. D., III.; van Opdenbosch, N. Validation of the general purpose Tripos 5.2 force field. *J. Comput. Chem.* **1989**, *10*, 982−1012.
(84) Pearlman, D. A.; Case, D. A.; Caldwell, J. W.; Ross, W. S.; Cheatham, T. E.; DeBolt, S.; Ferguson, D.; Seibel, G. L.; Kollman, P. A. AMBER, a package of computer programs for applying molecular mechanics, normal-mode analysis, molecular dynamics and free energy calculations to simulate the structural and energetic properties of molecules. *Comput. Phys. Commun.* **1995**, *91*, 1−41.
(85) Case, D. A.; Pearlman, D. A.; Caldwell, J. W.; Cheatham, T. E.; Wang, J.; Ross, W. S.; Simmerling, C. L.; Darden, T. A.; Merz, K. M.; Stanton, R. V.; Cheng, A. L.; Vincent, J. J.; Crowley, M.; Tsui, V.; Gohlke, H.; Radmer, R. J.; Duan, Y.; Pitera, J.; Massova, I.; Seibel, G. L.; Singh, U. C.; Weiner, P. K.; Kollman, P. A. AMBER 7. 2002; University of California, San Francisco.
(86) Cornell, W. D.; Cieplak, C. I.; Bayly, I. R.; Gould, I. R.; Merz, K. M.; Ferguson, D. M.; Spellmeyer, D. C.; Fox, T.; Caldwell, J. W.; Kollman, P. A. A second generation force field for the simulation of proteins, nucleic acids and organic molecules. *J. Am. Chem. Soc.* **1995**, *117*, 5179−5197.
(87) Jorgensen, W. L.; Chandrasekhar, J.; Madura, J.; Klein, M. L. Comparison of simple potential functions for simulating liquid water. *J. Chem. Phys.* **1983**, *79*, 926−935.
(88) Wang, J.; Cieplak, P.; Kollman, P. A. How well does a restrained electrostatic potential (RESP) model perform in calculating conformational energies of organic and biological molecules? *J. Comput. Chem.* **2000**, *21*, 1049−1074.
(89) Wang, J.; Wolf, R. M.; Caldwell, J. W.; Kollman, P. A.; Case, D. A. Development and testing of a general amber force field. *J. Comput. Chem.* **2004**, *25*, 1157−1174.
(90) Darden, T.; York, D.; Pedersen, L. Particle mesh Ewald: An *N*log(*N*) method for Ewald sums in large systems. *J. Chem. Phys.* **1993**, *98*, 10089−10092.
(91) Humphrey, W.; Dalke, A.; Schulten, K. VMD: Visual molecular dynamics. *J. Mol. Graphics* **1996**, *14*, 33−38.
(92) Tang, K. C.; Mariuza, R.; Coward, J. K. Synthesis and evaluation of some stable multisubstrate adducts as specific inhibitors of spermidine synthase. *J. Med. Chem.* **1981**, *24*, 1277−1284.

JM050555A